

Contents lists available at ScienceDirect

Petroleum Science

journal homepage: www.keaipublishing.com/en/journals/petroleum-science



Original Paper

Wave-induced flow of pore fluid in a cracked porous solid containing penny-shaped inclusions



Manjeet Kumari ^a, Virender ^b, Manjeet Kumar ^{c, *}

- ^a Dept. of Mathematics, M P College for Women, Mandi Dabwali, 125104, India
- ^b Dept. of Mathematics, Ramias College, University of Delhi, Delhi, 110007, India
- ^c Dept. of Mathematics, Dr. B R Ambedkar Govt. College, Dabwali, 125104, India

ARTICLE INFO

Article history: Received 1 September 2020 Accepted 5 March 2021 Available online 11 September 2021

Edited by Jie Hao

Keywords:
Cracked porous solid
Penny-shaped inclusions
Longitudinal waves
Phase velocity
Attenuation
Reflection coefficients

ABSTRACT

An aim of current study is to analyze the contribution of reflected longitudinal waves to wave-induced fluid flow (WIFF) in the cracked porous solid. Initially, we investigate the time harmonic plane waves in cracked porous solid by employing the mathematical model proposed by Zhang et al. (2019). The solution is obtained in form of the Christoffel equations. The solution of the Christoffel equations indicates that there exist four (three dilatational and one shear) waves. These waves are attenuated in nature due to their complex and frequency-dependent velocities. The reflection coefficients are calculated at the sealed pore stress-free surface of cracked porous solid for the incidence of P_1 and SV waves. It is found that three longitudinal waves contribute to WIFF and the contribution of these waves to the induced fluid in the cracked porous solid is analyzed using the reflection coefficients of these longitudinal waves. We analytically show that the fluid flow induced by these longitudinal waves is linked directly to their respective reflection coefficients. Finally, a specific numerical example is considered to discuss and to depict the impact of various parameters on the characteristics of propagation like phase velocity/ attenuation, reflection coefficients and WIFF of longitudinal waves.

© 2021 The Authors. Publishing services by Elsevier B.V. on behalf of KeAi Communications Co. Ltd. This is an open access article under the CC BY-NC-ND license (http://creativecommons.org/licenses/by-nc-nd/

4.0/).

1. Introduction

Most of the geological materials like reservoir rocks are generally heterogeneous and fractured or cracked. The pores and cracked/fractured space of these types of materials are mainly filled with water, gas or oil. When an elastic wave propagates through such materials, the pore pressure is developed on the mesoscopic-scale (huge than pore size but quite little than seismic wavelength) and it induces the fluid flow between more compliant parts (cracks/fractures) and stiffer portion (background pores) of the material. Such a flow mechanism is recognized as WIFF. The wave induced fluid flow is the leading contributor of wave attenuation and dispersion, which is hugely influenced by the pore structure, fluid properties and lithology (Yao et al., 1985; Müller et al., 2010; Quintal et al., 2011; Khalid and Ahmed, 2016). Therefore, the presence of pores and cracks in the rocks beneath the earth's crust significantly influences the propagation of elastic waves. Though,

* Corresponding author. E-mail address: manjit.msc@gmail.com (M. Kumar). cracks have extremely smaller aspect ratio as compared to pores like crack thickness is much smaller than its lateral size, yet distinct sizes, shapes, locations and orientations of the cracks are generally possible in different rocks. Earlier, several endeavors have been made to assimilate the cracks into the rock models and to explore their effects on the propagation characteristics of elastic waves. Eshelby (1957) and Walsh (1965) started these endeavors to explore the impact of cracks on the elastics properties of rocks containing cracks. Afterward, Nur (1972) and Aggarwal et al. (1973) elucidated the travel time deviations in terms of the alterations in dilatancy around the focal zone and the flow of pore fluid into the dilatancy-formed cracks. Garvin and Knopoff (1973, 1975a, b) approximated the wave velocities for elastic solids containing a dilute concentration of small cracks. O'Connell and Budiansky (1974) and Budiansky and O'Connell (1976) investigated the influence of cracks on the elastic properties of an isotropic elastic solid. Later, O'Connell and Budiansky (1977) analyzed the viscoelastic properties of cracked viscoelastic solids for full and partial saturation of cracks. Shapiro (2003) deduced the analytical relations for the elastic moduli of a cracked porous medium as a function of stiff porosity, compliant porosity and pressure though he did not

consider the shapes of cracks. David and Zimmerman (2011) introduced the elastic moduli of an isotropic solid for randomly distributed and randomly orientated spheroidal pores. In other studies (Cheng and Toksöz, 1979; Tran et al., 2008; David and Zimmerman, 2012), the fluid exchange between the cracks and porous environment is not contemplated. In these studies, they have estimated the pore aspect-ratio distribution from the pressure dependence of dry velocities. These models can only furnish the crack characteristics, but these do not narrate the attenuation and velocity dispersion mechanism. Most of these endeavors were based on the introduction of fluid-saturated cracks in elastic materials.

In most of the classical approaches, the well known Biot's poroelastic theory (1956a, b, 1962a, b) is employed to study the elastic wave exploration of earth's shallow crust. Biot's poroelastic theory considers the global-flow mechanism in saturated porous media and is equivalent to Gassmann (1951) in the low-frequency limit. However, it is not suitable to model the fluid flow between pores and cracks. Hence, several models by various researchers (Mavko and Nur, 1975; Murphy et al., 1986; Gurevich et al., 2009) have been proposed in the past few decades to address this local mechanism. Interestingly, both flow mechanisms coexist in a cracked porous medium. Mavko and Nur (1975) introduced the squirt flow mechanism for the fluid flow at pore scale level to explain the velocity dispersion/attenuation in the ultrasonic frequency band. Budiansky and O'Connell (1980) analyzed the local flow effects for penny-shaped cracks and spherical pores. Mayko and Nur (1979) and Dvorkin and Nur (1993) introduced the "squirt flow" theories to explain the local fluid flow. The later theory is often referred as the BISQ theory. But, two most important crack characteristics (crack density and aspect ratio) are not assimilated in BISQ theory. Tang (2011) and Tang et al. (2012) addressed these shortcomings in their model which is known as Tang model. They perceived that the relaxation frequency and amount of wave dispersion/attenuation are guarded by crack density and aspect ratio. Jakobsen et al. (2003) analyzed the effects of pores and cracks on the elastic behavior by considering an arbitrary distribution of pores and fractures based on the T-matrix approach. Pride et al. (2004) elucidated that the cracks can be treated as penny-shaped inclusions. Galvin and Gurevich (2009) analyzed the elastic wave dispersion and attenuation in a porous medium containing aligned sparsely distributed penny-shaped cracks. Yao et al. (2015) modeled the wave dispersion and attenuation by using the dynamic fluid modulus. They modified the original fluid modulus by introducing a flow term induced by the squirt flow into the original fluid modulus. Furthermore, Guo et al. (2017) investigated the relations between the elastic properties of rocks and intersecting fractures. Ba et al. (2015) developed a double double-porosity model to analyze the elastic wave propagation in porous media including both patchy saturation and fabric heterogeneity at different scales. They studied effects of pore fluid and solid frame heterogeneities on the dispersion/attenuation characteristics of elastic wave. Later, Ba et al. (2017) developed a double double-porosity model for rock anelasticity due to patchy saturation and fabric heterogeneity. They have studied the effects of fabric and saturation inhomogeneities on wave attenuation and velocity dispersion. Zhang et al. (2020) proposed the differential poroelasticity model to describe the wave propagation and dissipation in fluid-saturated rocks, which consists of infinite components.

WIFF is the main cause of attenuation and velocity dispersion in the fluid-saturated porous media, so keeping in view the importance of WIFF, recently Kumar and his co-workers (Kumar et al. 2018, 2019, 2019; Barak et al., 2018; Kumari et al., 2019) studied the impact of WIFF on the seismic waves propagation. Recently, Kumari and Kumar (2020) investigated the effects of propagation

direction, inhomogeneity parameter, pores characteristics, pore fluid viscosity, crack radius, crack density and local fluid flow (LFF) on the reflection characteristics of inhomogeneous waves at the surface of a cracked porous solid with penny-shaped inclusions. Zhang et al. (2019) introduced a mathematical model based on the Biot-Rayleigh theory developed by Ba et al. (2011) to investigate the wave motion in a cracked porous solid with penny-shaped inclusions. They formulated the governing equations assimilating most of the crack characteristics of cracked porous solid. They analyzed the influences of three key parameters (crack radius, crack density and aspect ratio) on the propagation characteristics (velocity/attenuation) of fast P and SV waves. In the present problem, we analyze the contribution of reflected longitudinal waves to WIFF in the cracked porous solid. For this purpose, we investigate the time harmonic plane waves in cracked porous solid by employing the mathematical model proposed by Zhang et al. (2019). The solution of the model is obtained in the form of the Christoffel equations. The solution of the Christoffel equations indicates that there exist three dilatational waves and one shear wave. These waves are attenuated in nature due to their complex and frequency-dependent velocities. These complex velocities are resolved in terms of the phase velocities and attenuation coefficients. The reflection coefficients are calculated at the sealed pore stress-free surface of cracked porous solid for the incidence of P_1 and SV waves. The contribution of three longitudinal waves to the induced fluid in the cracked porous solid is calculated using the reflection coefficients of these longitudinal waves. We analytically show that the fluid flow induced by these longitudinal waves is directly associated to their respective reflection coefficients. A specific numerical example is considered to discuss the impacts of various parameters on the propagation characteristics (phase velocity/attenuation), reflection coefficients and WIFF of longitudinal waves.

2. Basic equations

Following Zhang et al. (2019), the governing wave propagation equations, which assimilate most of the crack characteristics like crack radius, crack density, aspect ratio etc., of the cracked porous media with penny-shaped inclusions in absence of body forces are given by

$$\tau_{ij,j} = \rho \ddot{u}_i + \rho_f \ddot{v}_i + \rho_f \ddot{w}_i,$$

$$\left(-P_{f1}\right)_{,i} = \rho_f \ddot{u}_i + m_1 \ddot{v}_i + \frac{\eta}{\kappa_1} \frac{\Phi_{10}}{\Phi_1} \dot{v}_i,$$

$$\left(-P_{f2}\right)_{i} = \rho_f \ddot{u}_i + m_2 \ddot{w}_i + \frac{\eta}{\kappa_2} \frac{\Phi_{20}}{\Phi_2} \dot{w}_i, \tag{1}$$

where η is the fluid viscosity, $\kappa_1(\kappa_2)$ is the permeability of the host medium (inclusions), $\rho (= (1-\Phi)\rho_s + \Phi \rho_f)$ denotes the density of the porous aggregate, $\rho_f(\rho_s)$ is the density of pore fluid (grain). u_i, v_i , and w_i are the particle displacements of the rock frame, fluid in host medium, and fluid in inclusion, respectively. The dissipation coefficients m_1 and m_2 are defined as follows (Biot, 1962a).

$$m_k = \frac{\tau_k \rho_f}{\Phi_k}, \ (k = 1, \ 2),$$

where $\tau_1(\tau_2)$ defines the tortuosity of host medium (inclusions). $\Phi = \Phi_1 + \Phi_2$ is the total porosity of the considered medium, is consisting of host medium porosity $\Phi_1(=\nu_1\Phi_{10})$, and inclusions porosity $\Phi_2(=\nu_2\Phi_{20})$. $\nu_1(\nu_2)$ represents the volume fraction of host

medium (inclusions). $\Phi_{10}(\Phi_{20})$ denotes the local porosity of host medium (inclusions).

Following Zhang et al. (2019), the fluid variation (ς) described by the periodic cylindrical oscillations between the host porous frame and penny-shaped inclusions is given by

$$\varsigma = \frac{1}{\Phi_1} \left(1 - \frac{R_0^2}{R^2} \right),\tag{2}$$

where R denotes the radius of the penny-shaped inclusions after LFF

Zhang et al. (2019) derived the LFF governing equation by generalizing Rayleigh's theory (Rayleigh, 1917) and Biot poroelasticity theory (Biot, 1962a). With ς as a generalized coordinate, the Lagrange's equation for LFF is written as

$$\begin{split} &\left(\frac{3}{8} + \frac{\Phi_{20}}{2\Phi_{10}} \ln \frac{L + R_0}{R_0}\right) \Phi_1^2 \Phi_2 \rho_f R_0^2 \ddot{\varsigma} + \left(\frac{3\eta}{8\kappa_2} + \frac{\eta}{2\kappa_1} \ln \frac{L + R_0}{R_0}\right) \Phi_{20} \Phi_1^2 \Phi_2 \rho_f R_0^2 \dot{\varsigma} \\ &+ \frac{\eta}{2\kappa_1} \ln \frac{L + R_0}{R_0}\right) \Phi_{20} \Phi_1^2 \Phi_2 \rho_f R_0^2 \dot{\varsigma} \\ &= \Phi_1 \Phi_2 (\alpha_1 M_1 - \alpha_2 M_2) \nabla . \mathbf{u} + \Phi_1 \Phi_2 (M_1 \nabla . \mathbf{v} - M_2 \nabla . \mathbf{w}) \\ &+ \Phi_1^2 \Phi_2^2 (M_1 + M_2) \varsigma, \end{split} \tag{3}$$

where $L \sim \left(=\sqrt{\frac{R_0^2}{12}}\right)$ denotes the characteristic length of the fluid

flow and R_0 is the crack radius.

The stress-strain relations are given by

$$\tau_{ij} = (\lambda_c u_{k,k} + \alpha_1 M_1 v_{k,k} + \alpha_2 M_2 w_{k,k} + \Phi_1 \Phi_2 (\alpha_1 M_1 - \alpha_2 M_2) \varsigma) \delta_{ij} + \mu(u_{i,j} + u_{j,i}),$$

$$\left(-P_{f1}\right) = \left(\alpha_1 M_1 u_{k,k} + M_1 v_{k,k} + M_1 \Phi_1 \Phi_2 \varsigma\right) \delta_{ij},$$

$$(-P_{f2}) = (\alpha_2 M_2 u_{k,k} + M_2 w_{k,k} - M_2 \Phi_1 \Phi_2 \varsigma) \delta_{ij}, \tag{4}$$

where δ_{ij} is the Kronecker delta, τ_{ij} is the total stress, and P_{fm} are the pore-fluid pressures in each phase. μ denotes the shear modulus of rock (composite). The elastic constants are given by

denotes the shear modulus of solid grains. The porosity of cracks can be expressed as $\Phi_c=2\pi\epsilon\gamma^*$, where $\Phi_2=\Phi_c$. γ^* represents the crack aspect ratio. ϵ represents the crack density, and ν_B represents the Poisson's ratio. The dry bulk modulus of the host medium is given by (Pride et al., 2004) $K_{b1}=\frac{(1-\Phi_{10})K_s}{1+c_1\Phi_{10}}$, and dry modulus of inclusion is obtained from the relation $\frac{\nu_2}{K_{b2}}=\frac{1}{K_b}-\frac{\nu_1}{K_{b1}}$. c_1 is the consolidation parameter of host medium.

3. Harmonic plane waves

For time harmonic vibrations of the material particles ($\sim e^{-\iota \omega t}$) with angular frequency ω , equation (3) is solved as follows.

$$\varsigma = \lambda_0 \nabla . \mathbf{u} + \lambda_1 \nabla . \mathbf{v} + \lambda_2 \nabla . \mathbf{w},
(\lambda_0, \lambda_1, \lambda_2) = \left((\alpha_2 M_2 - \alpha_1 M_1, -M_1, M_2) \middle/ \left[(\Phi_1 \Phi_2) \right] \right)
\left(M_1 + M_2 + \omega^2 \varepsilon_1 \right) \right),$$
(5)

where
$$\varepsilon_1 = \left(\frac{3}{8} + \frac{\phi_{20}}{2\phi_{10}} ln \frac{L + R_0}{R_0}\right) \rho_f \frac{R_0^2}{\Phi_2} + \frac{\iota}{\omega} \left(\frac{3\eta}{8\kappa_2} + \frac{\eta}{2\kappa_1} ln \frac{L + R_0}{R_0}\right) \Phi_{20} \frac{R_0^2}{\Phi_2}.$$

The parameters λ_j , (j=0,1,2), in the above equation control the fluid flow ς between the host medium and inclusions. So, the absence of LFF is defined with $\lambda_0=\lambda_1=\lambda_2$.

Equations of motion in terms of the displacement components are as follows.

$$(a_0 + \mu)u_{j,ij} + a_1v_{j,ij} + a_2w_{j,ij} + \mu u_{i,jj} = \rho \ddot{u}_i + \rho_f \ddot{v}_i + \rho_f \ddot{w}_i,$$

$$b_0 u_{j,ij} + b_1 v_{j,ij} + b_2 w_{j,ij} = \rho_f \ddot{u}_i + m_1 \ddot{v}_i + \gamma_1 \dot{v}_i$$

$$c_0 u_{i,ij} + c_1 v_{i,ij} + c_2 w_{i,ij} = \rho_f \ddot{u}_i + m_2 \ddot{w}_i + \gamma_2 \dot{w}_i, \tag{6}$$

where
$$a_0 = \lambda_c + \lambda_0 \lambda_3$$
, $a_1 = \alpha_1 M_1 + \lambda_1 \lambda_3$, $a_2 = \alpha_2 M_2 + \lambda_2 \lambda_3$,

$$b_0 = M_1(\alpha_1 + \lambda_0 \Phi_1 \Phi_2), \ b_1 = M_1(1 + \lambda_1 \Phi_1 \Phi_2), \ b_2 = M_1 \Phi_1 \Phi_2 \lambda_2,$$

$$c_0 = M_2(\alpha_2 - \lambda_0 \Phi_1 \Phi_2), c_1 = -M_2 \lambda_1 \Phi_1 \Phi_2, c_2 = M_2(1 - \Phi_1 \Phi_2 \lambda_2),$$

$$\begin{split} &\lambda_{\text{C}} = (1-\Phi)K_{\text{S}} - \frac{2}{3}\mu + \left(2 - \frac{K_{\text{S}}}{K_{\text{f}}}\right)(\alpha_{1}\Phi_{1}M_{1} + \alpha_{2}\Phi_{2}M_{2}) - \left(1 - \frac{K_{\text{S}}}{K_{\text{f}}}\right)\left(\Phi_{1}^{2}M_{1} + \Phi_{2}^{2}M_{2}\right), \\ &\alpha_{1} = \frac{\beta\Phi_{1}K_{\text{S}}}{\gamma K_{\text{f}}} + \Phi_{1}, \ \alpha_{2} = \frac{\Phi_{2}K_{\text{S}}}{\gamma K_{\text{f}}} + \Phi_{2}, \ M_{1} = \frac{K_{f}}{\left(\frac{\beta}{\gamma} + 1\right)\Phi_{1}}, \ M_{2} = \frac{K_{f}}{\left(\frac{1}{\gamma} + 1\right)\Phi_{2}}, \ \gamma = \frac{K_{\text{S}}}{K_{\text{f}}}\left(\frac{\beta\Phi_{1} + \Phi_{2}}{1 - \Phi - \frac{K_{b}}{K_{\text{S}}}}\right), \\ &\beta = \frac{\Phi_{20}}{\Phi_{10}}\left(\frac{1 - (1 - \Phi_{10})\frac{K_{\text{S}}}{K_{b1}}}{1 - (1 - \Phi_{20})\frac{K_{\text{S}}}{K_{b2}}}\right), \ K_{b} = \frac{2}{3}\left(\frac{1 + \nu_{B}}{1 - 2\nu_{B}}\right)\mu_{b}, \ \mu_{b} = \mu_{\text{S}}\left(1 - \frac{\Phi}{1 - b_{B}} - B_{B}\varepsilon\right), \\ &b_{B} = \frac{2}{15}\left(\frac{4 - 5\nu_{B}}{1 - \nu_{B}}\right), \ B_{B} = \frac{32}{45}\left(\frac{(1 - \nu_{B})(5 - \nu_{B})}{2 - \nu_{B}}\right), \end{split}$$

$$\lambda_3 = \Phi_1 \Phi_2(\alpha_1 M_1 - \alpha_2 M_2), \ \ \gamma_1 = \frac{\eta}{\kappa_1} \frac{\Phi_{10}}{\Phi_1}, \ \ \gamma_2 = \frac{\eta}{\kappa_2} \frac{\Phi_{20}}{\Phi_2}.$$

Then, to obtained the solution of (6), the displacement components are taken as

$$(u_i, v_i, w_i) = (A_i, B_i, C_i)e^{i\omega(s_k x_k - t)}, j = 1, 2, 3,$$
(7)

where $\mathbf{s} = (s_1, s_2, s_3)$ denotes the slowness vector. The vectors $\mathbf{A} = (A_1, A_2, A_3)^T$, $\mathbf{B} = (B_1, B_2, B_3)^T$, and $\mathbf{C} = (C_1, C_2, C_3)^T$, define, respectively, the polarizations for the motions of solid particles and fluid particles in two porous volumes (i.e., host medium and inclusions). The dual (complex) vector $(s_1, s_2, s_3) = (n_1, n_2, n_3)/V$ represents the propagation/attenuation of a wave through a unit vector (n_1, n_2, n_3) and a velocity V. By substituting (7) in (6), we can obtain a system of nine equations, given by

$$\left[(a_0 + \mu) n_i n_j - \left(\mu - \rho V^2 \delta_{ij} \right) \right] \times \left[A_j + \left[a_1 n_i n_j - \rho_f V^2 \delta_{ij} \right] B_j + \left[a_2 n_i n_j - \rho_f V^2 \delta_{ij} \right] C_j = 0,$$
(8)

$$\begin{split} & \left[b_0n_in_j-\rho_fV^2\delta_{ij}\right]A_j+\left[b_1n_in_j-\rho_1V^2\delta_{ij}\right]B_j\\ &+\left[b_2n_in_j\right]C_j=0,\;\rho_1=m_1+\frac{\iota}{\omega}\gamma_1, \end{split} \tag{9}$$

$$\left[c_{0}n_{i}n_{j}-\rho_{f}V^{2}\delta_{ij}\right]A_{j}+\left[c_{1}n_{i}n_{j}\right]B_{j}+\left[c_{2}n_{i}n_{j}-\rho_{2}V^{2}\delta_{ij}\right]C_{j}=0,
\rho_{2}=m_{2}+\frac{\iota}{\omega}\gamma_{2}.$$
(10)

With the help of equations (9) and (10), we can find two relations, given by

$$B_{i} = \Gamma_{ij}A_{j}, \quad \Gamma = \frac{f_{0}}{e_{0}}\left(\mathbf{I} - \mathbf{n}^{T}\mathbf{n}\right) + \frac{f_{0}V^{4} + f_{1}V^{2} + f_{2}}{e_{0}V^{4} + e_{1}V^{2} + e_{2}}\mathbf{n}^{T}\mathbf{n}, \tag{11}$$

$$C_i = \Theta_{ij}A_j, \quad \Theta = \frac{g_0}{e_0} \left(\mathbf{I} - \boldsymbol{n}^T \boldsymbol{n} \right) + \frac{g_0V^4 + g_1V^2 + g_2}{e_0V^4 + e_1V^2 + e_2} \boldsymbol{n}^T \boldsymbol{n},$$
 (12)

where, $e_2 = b_1c_2 - b_2c_1$, $e_1 = -b_1\rho_2 - c_2\rho_1$, $e_0 = \rho_1\rho_2$,

$$f_2 = b_2c_0 - b_0c_2$$
, $f_1 = b_0\rho_2 + \rho_f(c_2 - b_2)$, $f_0 = -\rho_2\rho_f$,

$$g_2 = b_0c_1 - b_1c_0$$
, $g_1 = c_0\rho_1 + \rho_f(b_1 - c_1)$, $g_0 = -\rho_1\rho_f$.

On applying equations (11) and (12) in (8), we obtained a Christoffel system, and is given by

$$D_{ij}A_i = 0, \quad \mathbf{D} = a_3 \mathbf{n}^T \mathbf{n} + b_3 (\mathbf{I} - \mathbf{n}^T \mathbf{n}), \tag{13}$$

where, $a_3 = a_0 + 2\mu - \rho V^2 + (a_1$

$$-\rho_f V^2 \bigg) \frac{f_0 V^4 + f_1 V^2 + f_2}{e_0 V^4 + e_1 V^2 + e_2} + \bigg(a_2 - \rho_f V^2 \bigg) \frac{g_0 V^4 + g_1 V^2 + g_2}{e_0 V^4 + e_1 V^2 + e_2},$$

$$b_3 = \mu - V^2 \left(\rho + \rho_f \left(\frac{f_0 + g_0}{e_0} \right) \right)$$
, **I** is the third order identity matrix

and \boldsymbol{n}^T represents the transpose of the row-matrix $\boldsymbol{n}=(n_1,n_2,n_3)$.

The non-trivial solution of system of equation (13) demonstrates the existence of four (three longitudinal and one shear) waves in the cracked porous solid with penny-shaped inclusions. The nontrivial solution of (13) is ensured by vanishing the determinant $(=a_3b_3^2)$ of the matrix $a_3{\bf n}^T{\bf n}+b_3({\bf l}-{\bf n}^T{\bf n})$. Therefore, the previous system is algebraically translated into two sub-systems, which produce the dynamics of wave propagation in the cracked porous solid.

The first one (i.e. $a_3 = 0$) implies that

$$D_3V^6 + D_2V^4 + D_1V^2 + D_0 = 0, (14)$$

where

$$D_3 = -\left[\rho e_0 + \rho_f(f_0 + g_0)\right],$$

$$D_2 = \left[(a_0 + 2\mu)e_0 + a_1f_0 + a_2g_0 - \rho e_1 - \rho_f(f_1 + g_1) \right],$$

$$D_1 = \left\lceil (a_0 + 2\mu)e_1 + a_1f_1 + a_2g_1 - \rho e_2 - \rho_f(f_2 + g_2) \right\rceil,$$

$$D_0 = [(a_0 + 2\mu)e_2 + a_1f_2 + a_2g_2].$$

As the coefficients D_j in (14) are complex due to the ubiquity of viscous fluid in both host medium and inclusions, so their roots are also complex. Therefore, three complex roots of the previous equation demonstrate the existence of three attenuated waves in the present medium. From equation (13), it is found that the polarization vector (A_1, A_2, A_3) , is parallel to \mathbf{n} , so these waves are called longitudinal waves. These waves, with velocities defined by V_j , (j=1, 2, 3), are named as P_1, P_2, P_3 waves, respectively.

Another condition (i.e. $b_3 = 0$) yields

$$\mu - V^2 \left(\rho + \rho_f \left(\frac{f_0 + g_0}{e_0} \right) \right) = 0. \tag{15}$$

Corresponding to this condition, it founds that the polarization vector (A_1, A_2, A_3) , parallel to the row or column of the symmetric matrix $(\mathbf{I} - \boldsymbol{n}^T \boldsymbol{n})$. Therefore, the solution of equation (15) demonstrates the existence of lone transverse wave propagating with

complex velocity
$$V_4 = \sqrt{\mu/\left(
ho +
ho_f\left(rac{f_0 + g_0}{e_0}
ight)
ight)}$$
 in the considered

medium. Finally, we have four attenuated waves propagating in a dissipative cracked porous solid with penny-shaped inclusions. For each of these waves, the complex velocity is resolved as $V = V_R + \iota V_I$, to define the phase velocity $\alpha = |V|^2/V_R$ and attenuation coefficient $\beta = -2V_I/V_R$.

Plunging (11) and (12) into equation (7), the displacements of fluid particles in the host medium and penny-shaped inclusions for three longitudinal waves are found to be function of displacement

Table 1Values of dynamical and elastic constants of the cracked porous rock (Tang et al., 2012).

Property Value	
K _s (GPa)	37.9
μ_{s} (GPa)	32.6
K_f (GPa)	2.5
$\rho_{\rm s}~({\rm kg/m^3})$	2650
$\rho_f (kg/m^3)$	1000
$\eta(Pa.s)$	0.001
Φ_{10}	0.25
Φ_{20}	0.35
$\kappa_1(Darcy)$	0.1
$\kappa_1(Darcy)$	100
c_1	11
τ_1	2.4
τ_2	1

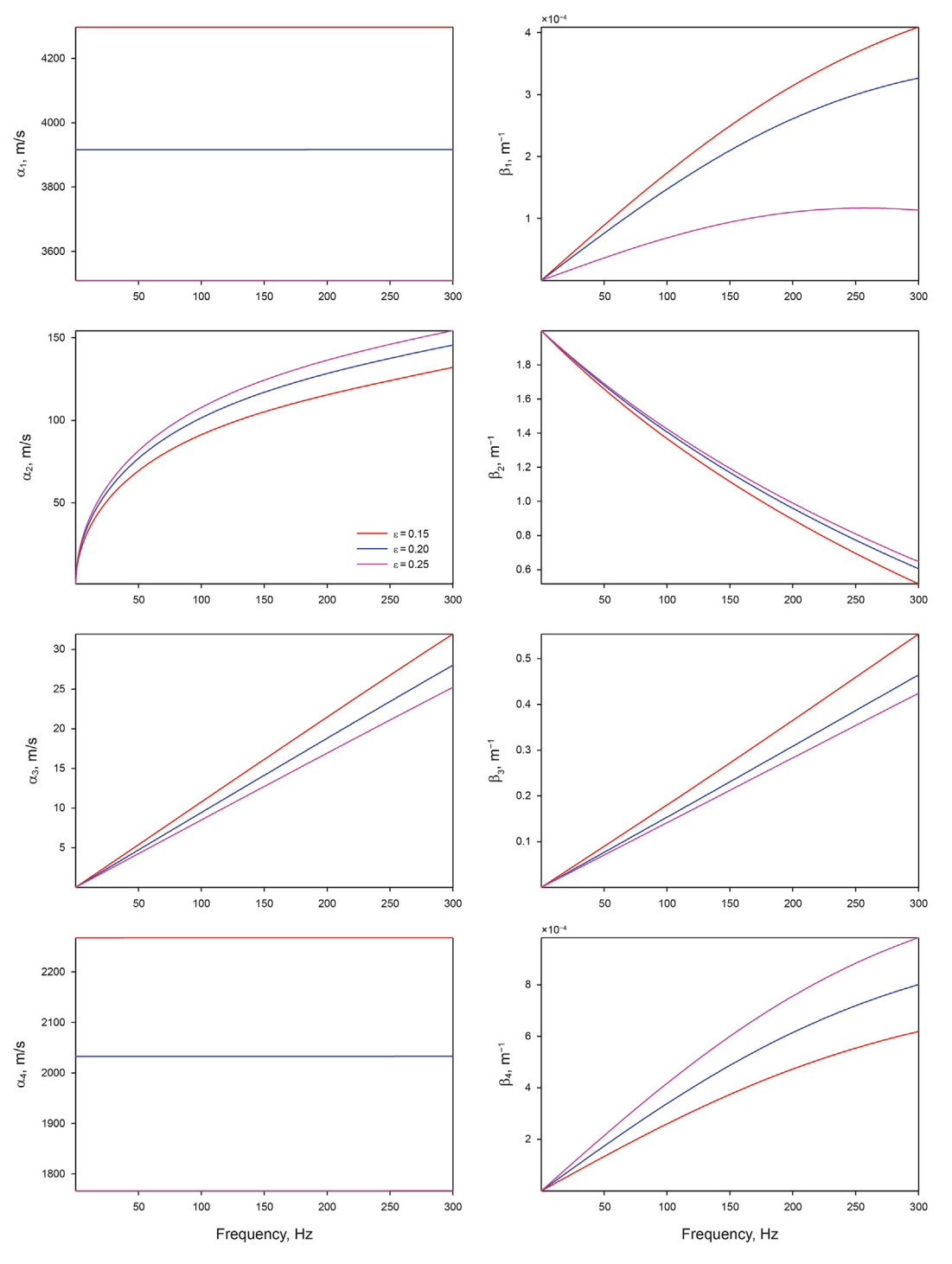


Fig. 1. Effect of crack density (ε) on the phase velocities $(\alpha_1, \alpha_2, \alpha_3, \alpha_4)$ and attenuation coefficients $(\beta_1, \beta_2, \beta_3, \beta_4)$ of P_1, P_2, P_3 , SV waves, respectively; $R_0 = 0.005 \text{m}$; $\gamma^* = 0.003$; $\nu_b = 0.3$.

of solid particles and which are given by

$$\label{eq:varphi} \pmb{v} = \Gamma(V), \quad \Gamma(V) = \frac{f_0 V^4 + f_1 V^2 + f_2}{e_0 V^4 + e_1 V^2 + e_2},$$

$${m w} = \Theta(V), \quad \Theta(V) = rac{g_0 V^4 + g_1 V^2 + g_2}{e_0 V^4 + e_1 V^2 + e_2}.$$

In the same manner, the displacements of fluid particles in the host medium and penny-shaped inclusions for transverse wave are also found to be function of displacement of solid particles and which are given by

$$v_j = \frac{f_0}{e_0} u_j, \quad w_j = \frac{g_0}{e_0} u_j, \quad (j = 1, 2, 3).$$
 (17)

(16)

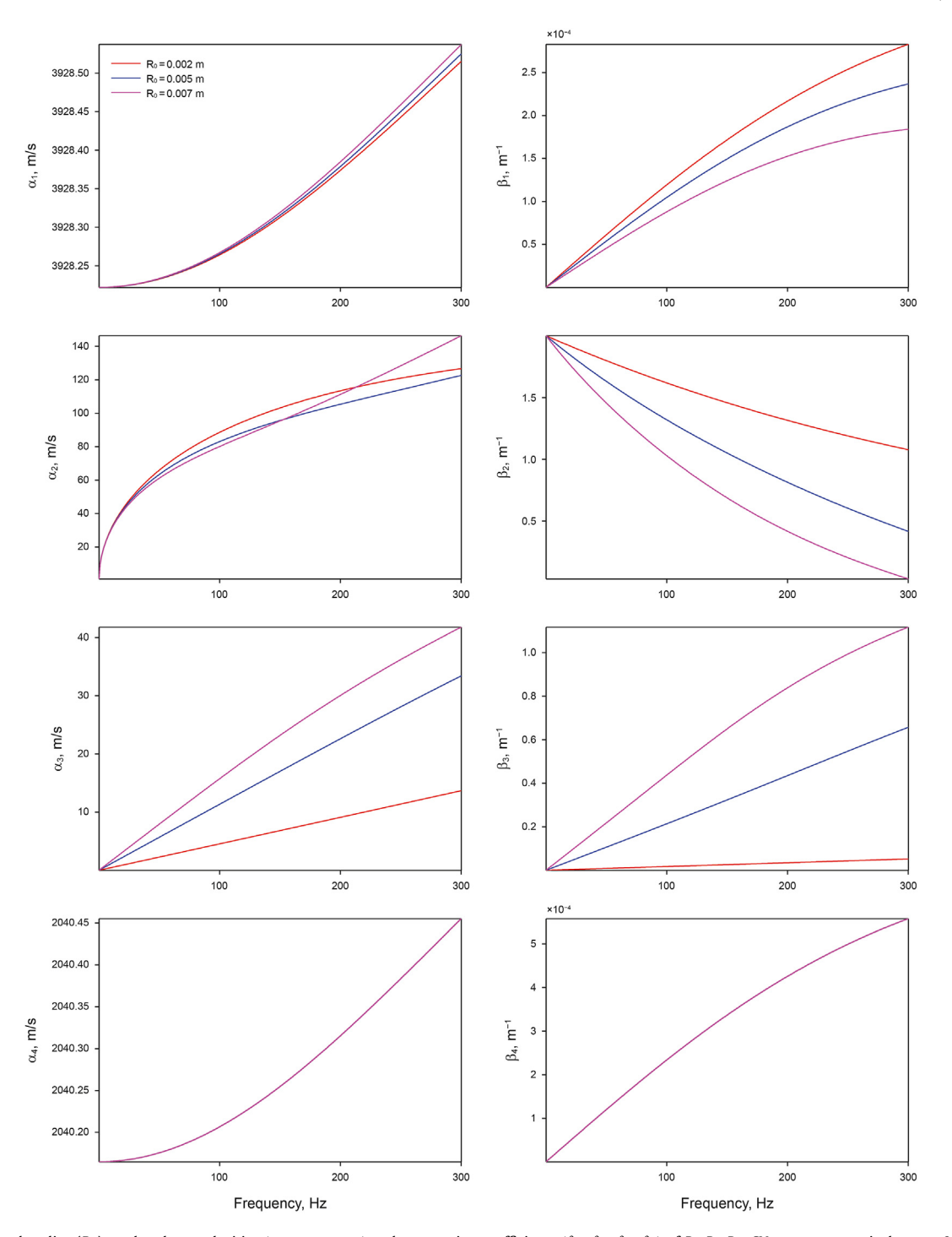


Fig. 2. Effect of crack radius (R_0) on the phase velocities (α_1 , α_2 , α_3 , α_4) and attenuation coefficients (β_1 , β_2 , β_3 , β_4) of P_1 , P_2 , P_3 , SV waves, respectively; $\varepsilon = 0.2$; $\gamma^* = 0.002$; $\nu_b = 0.3$.

4. Formulation of the problem

As our plan is to analyze the contribution of reflected longitudinal waves to the induced fluid flow in the cracked porous solid for the occurrence of P_1 and SV waves, we have considered a cracked porous half-space for this purpose. A train of longitudinal P_1 (or shear SV) waves is engendered at infinity and is pointed obliquely at the sealed pore stress-free surface of cracked porous solid.

4.1. Geometry of the problem

In rectangular Cartesian coordinate system (x_1,x_2,x_3) , cracked porous solid occupies the region $x_3 > 0$, bounded by the horizontal plane $x_3 = 0$. In the present problem, we have considered the wave motion in x_1x_3 -plane. In this plane, a plain inhomogeneous $(P_1$ or SV) wave with velocity V_0 and angular frequency ω is striking the boundary surface $x_3 = 0$ obliquely at an angle θ with normal to the free surface. Consequently, four inhomogeneous waves (P_1, P_2, P_3, P_3)

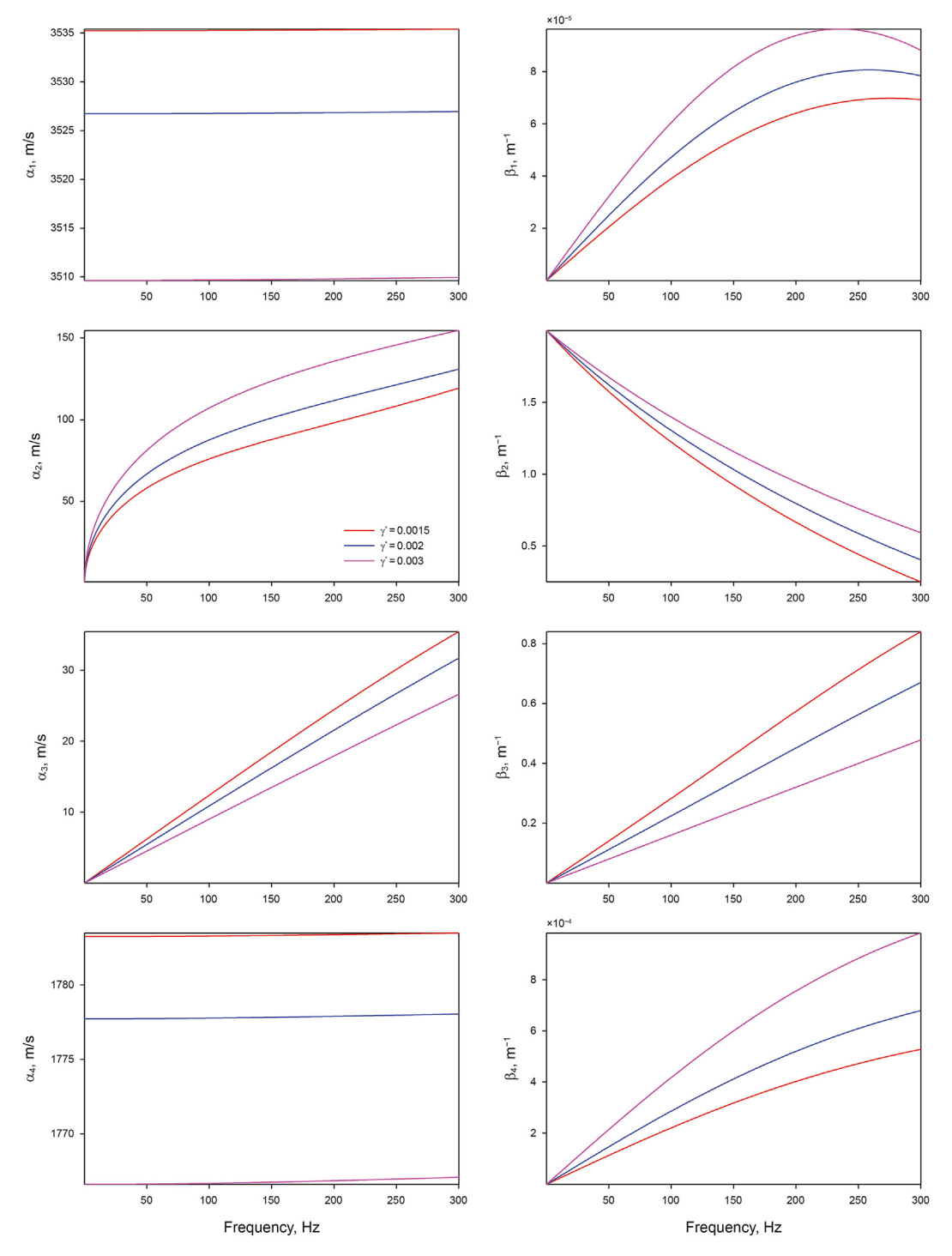


Fig. 3. Effect of crack aspect ratio (γ^*) on the phase velocities (α_1 , α_2 , α_3 , α_4) and attenuation coefficients (β_1 , β_2 , β_3 , β_4) of P_1, P_2, P_3 , SV waves, respectively; $\epsilon=0.25$; $R_0=0.0053$ m; $\nu_b=0.3$.

SV) are generated in the cracked porous solid.

4.2. Displacements

The cracked porous solid behaves dissipative due to the ubiquity of viscous fluids in both host medium and penny-shaped inclusions. Therefore, all the incident and reflected waves in the considered medium are attenuated. The conception of attenuated

waves has been completely explained in details by Kumar and Sharma (2013). The horizontal slowness of incident wave is given by (Borcherdt, 2009)

$$s = (|\mathbf{P}_0|/\omega)\sin\theta - \iota(|\mathbf{A}_0|/\omega)\sin(\theta - \gamma_0), \tag{18}$$

in which

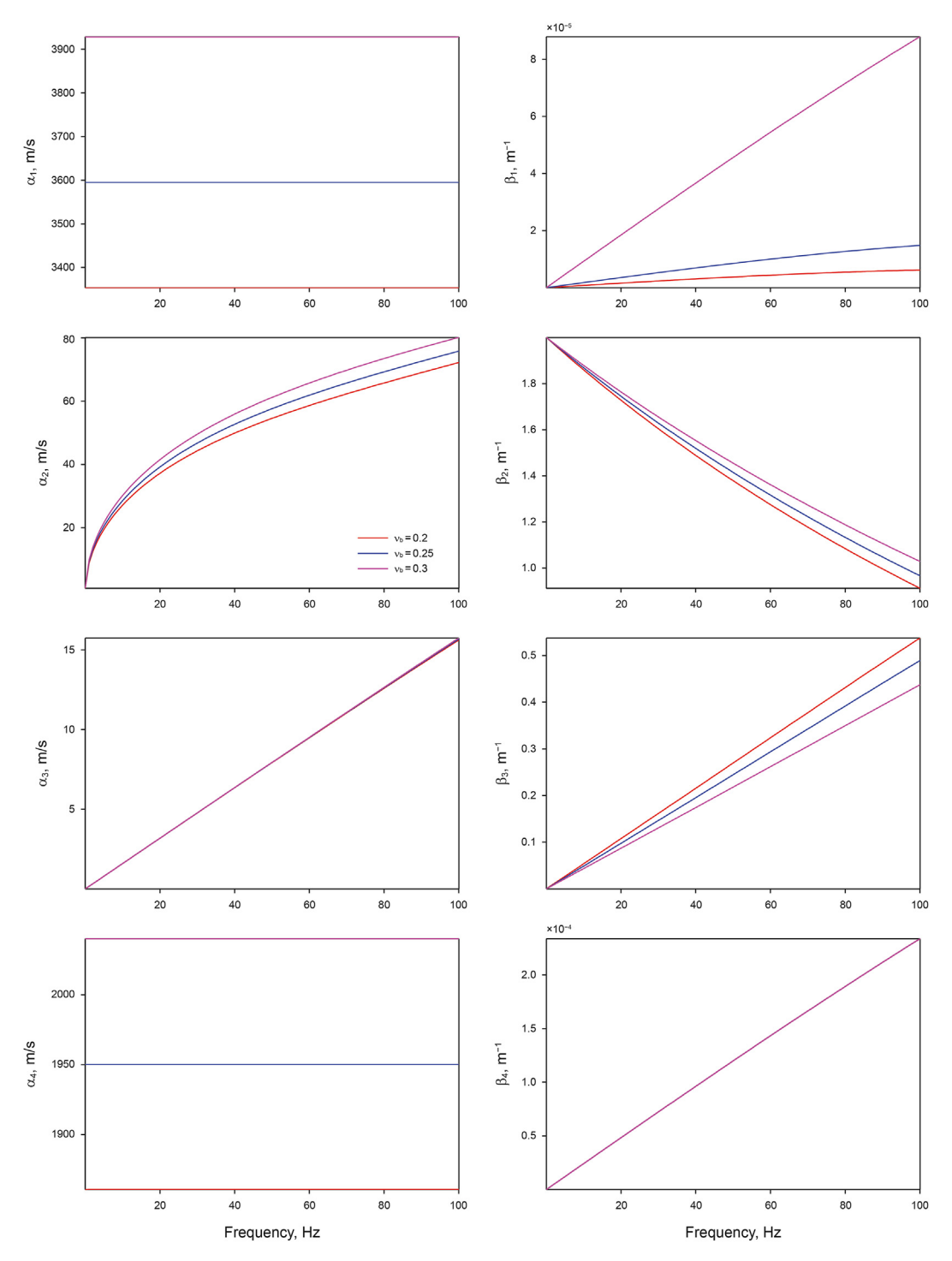


Fig. 4. Effect of Poisson's ratio (v_b) on the phase velocities (α_1 , α_2 , α_3 , α_4) and attenuation coefficients (β_1 , β_2 , β_3 , β_4) of P_1 , P_2 , P_3 , SV waves, respectively; $\varepsilon=0.2$; $R_0=0.007$ m; $\gamma^*=0.002$.

$$|\mathbf{P}_{0}| = \sqrt{\frac{1}{2} \left[\Re\left(\frac{\omega^{2}}{V_{0}^{2}}\right) + \sqrt{\left(\Re\left(\frac{\omega^{2}}{V_{0}^{2}}\right)\right)^{2} + \left(\Im\left(\frac{\omega^{2}}{V_{0}^{2}}\right) \middle/ \cos\gamma_{0}\right)^{2}} \right]}, \qquad |\mathbf{A}_{0}| = \sqrt{\frac{1}{2} \left[-\Re\left(\frac{\omega^{2}}{V_{0}^{2}}\right) + \sqrt{\left(\Re\left(\frac{\omega^{2}}{V_{0}^{2}}\right)\right)^{2} + \left(\Im\left(\frac{\omega^{2}}{V_{0}^{2}}\right) \middle/ \cos\gamma_{0}\right)^{2}} \right]}, \tag{19}$$

where θ denotes the angle of occurrence. P_0 (A_0) represents the

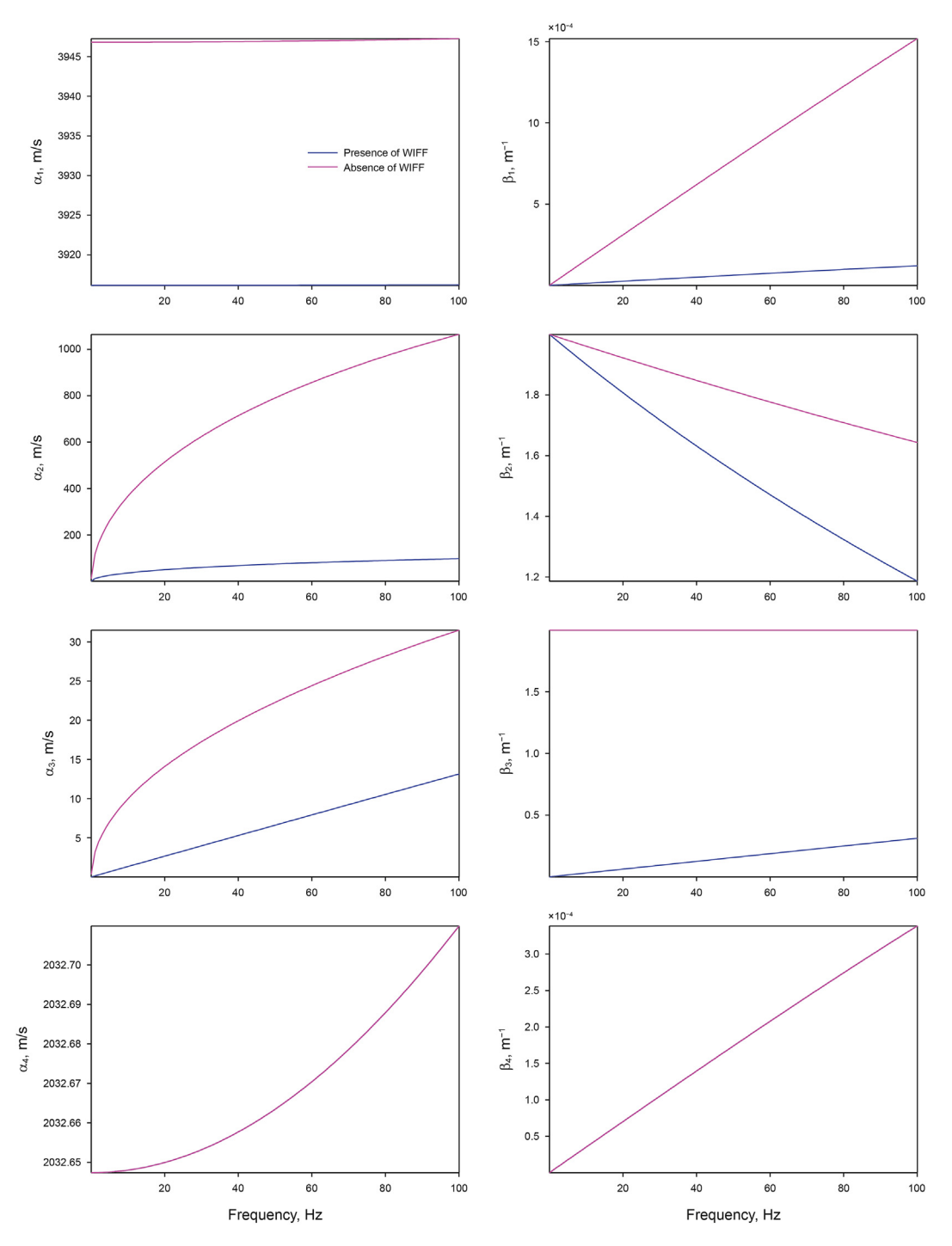


Fig. 5. Effect of WIFF on the phase velocities $(\alpha_1, \alpha_2, \alpha_3, \alpha_4)$ and attenuation coefficients $(\beta_1, \beta_2, \beta_3, \beta_4)$ of P_1, P_2, P_3 , SV waves, respectively; $\varepsilon = 0.2$; $R_0 = 0.007$ m; $\gamma^* = 0.003$; $\nu_b = 0.3$.

propagation (attenuation) vector. γ_0 denotes the angle of attenuation betwixt propagation vector and attenuation vector. V_0 identifies the velocity of incident wave.

The general displacement of material particles in x_1x_3 -plane associated with incident/reflected waves is defined as

$$\left(u_j, v_j, w_j\right) = (1, \Gamma_0, \Theta_0) A_j^{(0)} e^{\iota \omega (sx_1 + q_0x_3 - t)}$$

$$+\sum_{k=1}^{4} Z_k A_j^{(k)} (1, \Gamma_j, \Theta_j) e^{\iota \omega (s x_1 + q_j x_3 - t)}, j = 1, 3,$$
(21)

where, values 1 to 4 of index k identify the reflected P_1, P_2, P_3 and SV waves, respectively. The index '0' denotes the incident wave, so that $V_0 = V_k$ and $q_0 = -q_k$ denote the incident wave which is

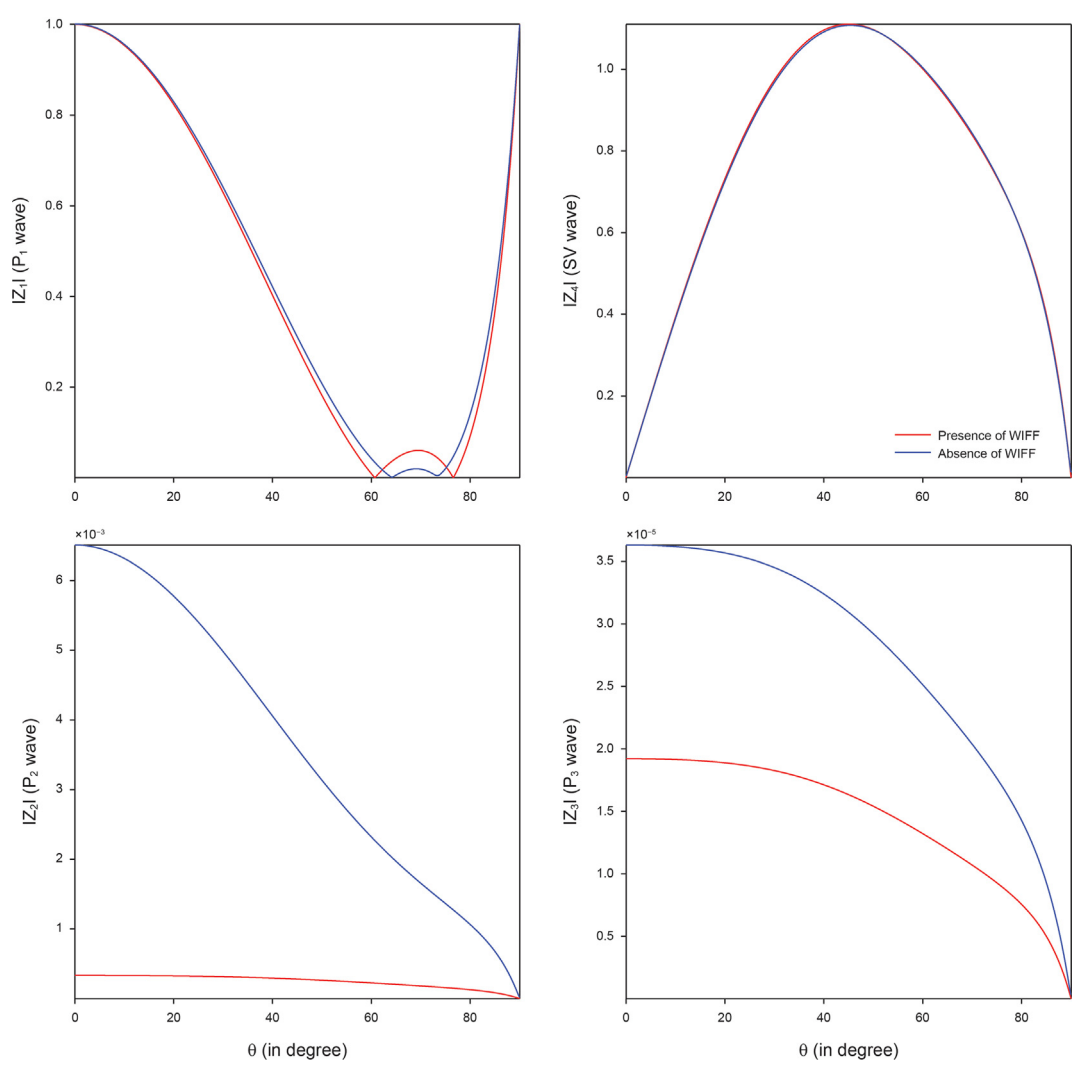


Fig. 6. Amplitude ratios $(|Z_1|, |Z_2|, |Z_3|, |Z_4|)$ of reflected waves; $\omega = 2\pi \times 300$ Hz; $\varepsilon = 0.15, R_0 = 0.0053$ m; $\gamma^* = 0.003; \nu_b = 0.3; \gamma_0 = 45^0;$ Incident P_1 wave.

recognized with index 'k'. The (Z_k) is the relative excitation factor of reflected waves. Here, $\Gamma_k = \Gamma(V_k)$, $\Theta_k = \Theta(V_k)$, (k=1,2,3), for longitudinal waves and $\Gamma_4 = \frac{f_0}{e_0}$, $\Theta_4 = \frac{g_0}{e_0}$, for shear wave. The horizontal slowness of each reflected waves is same as that of the incident wave (Snell's law). The vertical slowness of reflected waves

is defined as
$$q_k = \sqrt{\left(\frac{1}{V_k^2} - s^2\right)}$$
, $k = 1, 2, 3, 4$. In the x_1x_3 -plane,

the polarization vectors $(A_1^{(k)},0,A_3^{(k)})$ of the reflected *P*-waves are calculated as $(A_1^{(k)},0,A_3^{(k)})=(s,0,\ q_k)V_k,\ (k=1,\ 2,\ 3),$ and for the transverse wave is calculated as $(A_1^{(4)},0,A_3^{(4)})=(q_4,0,\ -s)V_4.$

4.3. Boundary conditions

Boundary conditions are steamed from the physical situations exist there to solve a specific problem. In the present problem, boundary conditions are considered at the stress-free surface $x_3 = 0$. Stress-free surface means both normal as well as tangential stresses should be vanished at that surface. We have assumed

sealed surface so as to preclude the release of pore-fluids from host medium to inclusions and vice-versa. In case of fully sealed pores boundary surface, discharge of fluid is not allowed out of aggregate. Hence, the boundary conditions at the surface $x_3 = 0$ with sealed pores and fractures are given by

i)
$$\tau_{33} = 0$$
,

$$ii) \tau_{31} = 0,$$

$$iii) \dot{v}_3 = 0,$$

$$iv) \dot{w}_3 = 0. \tag{22}$$

4.4. Reflection

In terms of four unknown (Z_1, Z_2, Z_3, Z_4) , the boundary conditions in (22) are transformed into a system of four simultaneous non-

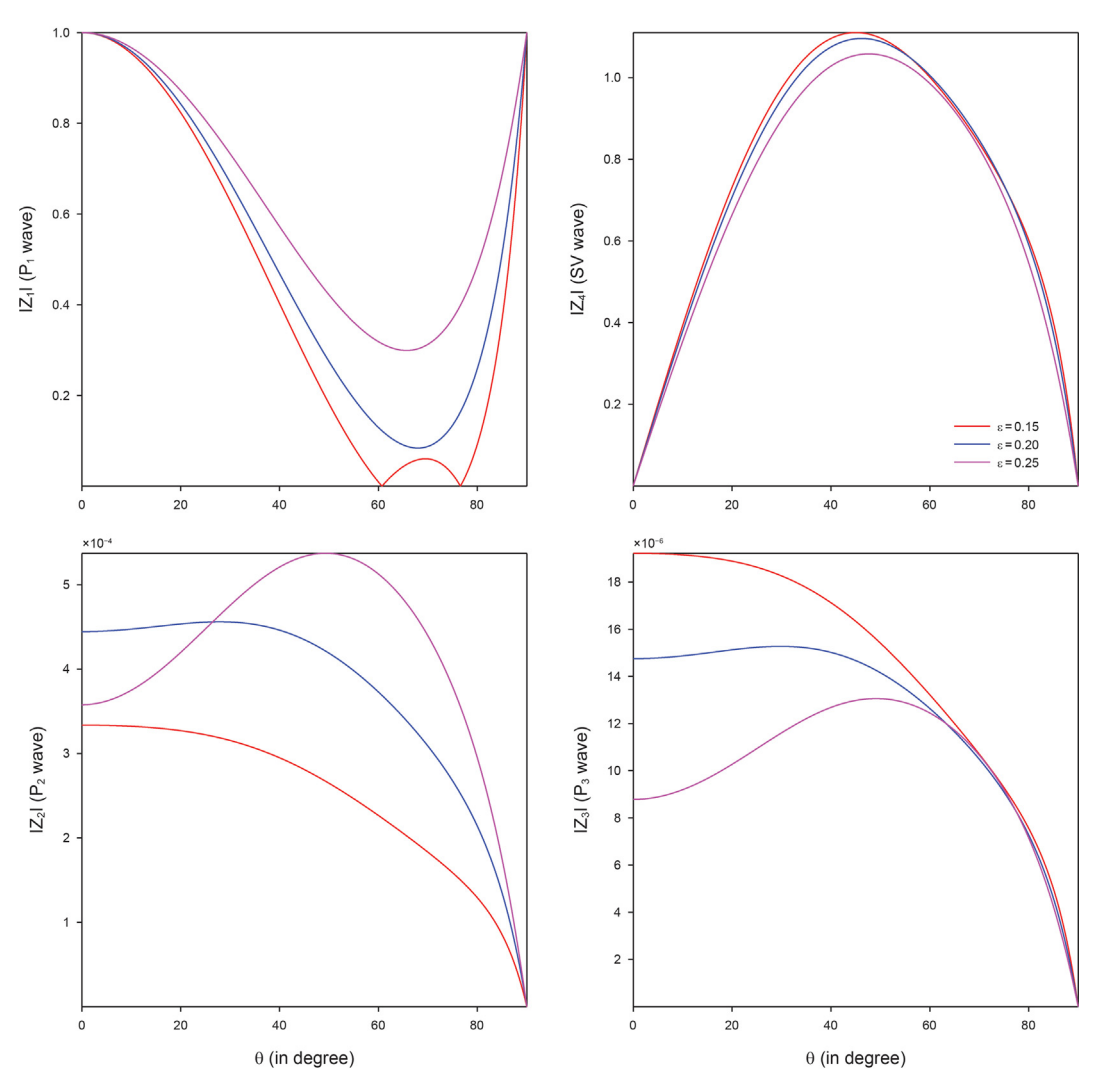


Fig. 7. Amplitude ratios $(|Z_1|, |Z_2|, |Z_3|, |Z_4|)$ of reflected waves; $\omega = 2\pi \times 300$ Hz; $R_0 = 0.0053$ m; $\gamma^* = 0.003$; $r_b = 0.3$; $\gamma_0 = 45^0$; Incident P_1 wave.

homogeneous linear equations which is given by

$$\sum_{i=1}^{4} G_{ij}Z_{j} = H_{i}, \ (i=1, 2, 3, 4), \tag{23}$$

where the coefficients $G_{ij},\ (i=1,\ 2,\ 3,\ 4;j=1,\ 2,\ 3,\ 4),$ are expressed as follows

$$G_{1j} = (a_0 + a_1\Gamma_j + a_2\Theta_j)(sA_1^{(j)} + q_jA_3^{(j)}) + 2\mu q_jA_3^{(j)},$$

$$G_{2j} = \mu \left(s A_3^{(j)} + q_j A_1^{(j)} \right),$$

$$G_{3j} = \Gamma_j A_3^{(j)},$$

$$G_{4j} = \Theta_j A_3^{(j)}.$$

The residues H_i in system (23) for incident $P_1(SV)$ wave is

written as follows:

$$\begin{split} H_1 &= -\,G_{11}(-G_{14}), H_2 = -\,G_{21}(-G_{24}), \; H_3 = -\,G_{31}(-G_{34}), \\ H_4 &= -\,G_{41}(-G_{44}). \end{split}$$

Using Gauss elimination method, the system of equation (23) is solved numerically for complex unknowns Z_j s.

4.5. Wave-induced fluid flow

Using the relations (16)-(17) in (5), the WIFF in pores can only be found as a function of dilation of solid particles and is defined as follows:

$$\varsigma = [\lambda_0 + \lambda_1 \Gamma(V) + \lambda_2 \Theta(V)] (u_{1,1} + u_{3,3}).$$
 (24)

Using equation (21) in the previous equation, we obtained

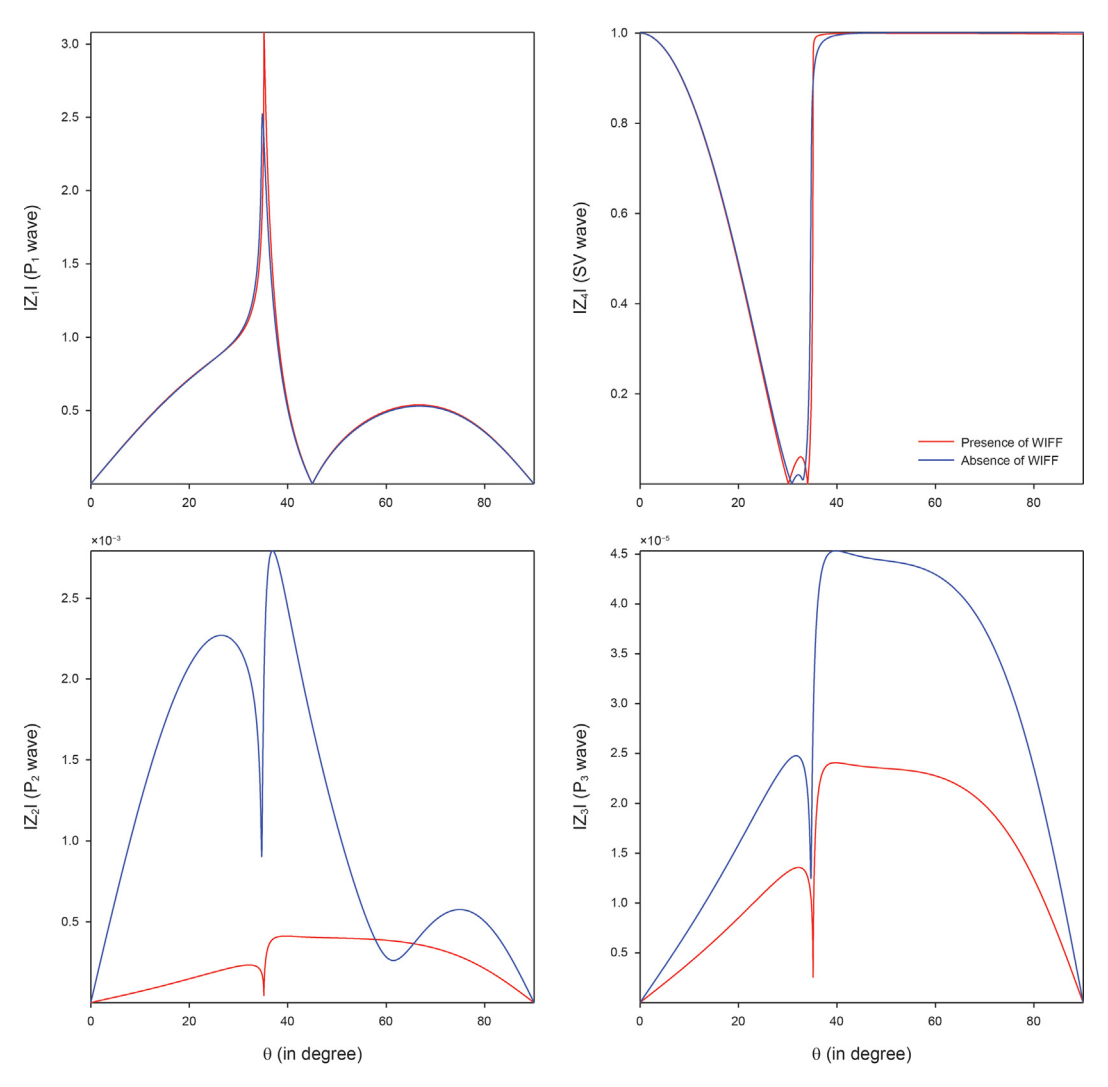


Fig. 8. Amplitude ratios $(|Z_1|, |Z_2|, |Z_3|, |Z_4|)$ of reflected waves; $\omega = 2\pi \times 300$ Hz; $\varepsilon = 0.15$; $R_0 = 0.0053$ m; $\gamma^* = 0.003$; $\nu_b = 0.3$; $\gamma_0 = 45^0$; Incident SV wave.

$$\varsigma(V_{k}) = \iota \omega Z_{k} [\lambda_{0} + \lambda_{1} \Gamma(V_{k}) + \lambda_{2} \Theta(V_{k})]
\times \left(s A_{1}^{(k)} + q_{k} A_{3}^{(k)} \right) e^{\iota \omega \left(s x_{1} + q_{j} x_{3} - t \right)},
(k = 1, 2, 3, 4).$$
(25)

If we assimilate the existence condition of shear wave in the above equation, then we can check that $\varsigma(V_4)=0$. It implies that WIFF in pores is controlled by three longitudinal waves. Therefor, $\varsigma(V_1),\ \varsigma(V_2),\ \varsigma(V_3)$ define the contributions of P_1,P_2,P_3 waves, respectively, to the total fluid flow. As V_k is complex, so is $\varsigma(V_k)$. Being a physical quantity, the fluid flow induced by longitudinal waves (i.e., ς_k) is calculated as a real part of its complex form ($\varsigma_k=\Re(\varsigma(V_k))$). The quantity $\varsigma_1+\varsigma_2+\varsigma_3$ defines the total fluid flow induced in the cracked porous solid due to the incidence of P_1 (or SV) wave at the stress-free surface of cracked porous solid with penny-shaped inclusions.

5. Numerical example

A sandstone (cracked porous solid), which is constituted by

high-porosity high-permeability penny-shaped inclusions and low-porosity low-permeability host medium, is considered for numerical purpose. The values of dynamical and elastic constants of the cracked porous rock used for numerical purpose are given in Table 1.

6. Numerical discussion

6.1. Effect of various parameters on the velocity and attenuation

The numerical example explains the impact of key parameters of cracks, WIFF and Poisson's ratio on the wave propagation characteristics (velocity/attenuation). The phase velocities $(\alpha_1, \alpha_2, \alpha_3, \alpha_4)$ and attenuation coefficients $(\beta_1, \beta_2, \beta_3, \beta_4)$ of P_1, P_2, P_3 , SV waves are computed with frequency ω for distinct parameters are exhibited in Figs. 1–5.

Fig. 1 exhibits the variations of phase velocities $(\alpha_1, \alpha_2, \alpha_3, \alpha_4)$ and attenuation coefficients $(\beta_1, \beta_2, \beta_3, \beta_4)$ of P_1, P_2, P_3 , SV waves with frequency for three different values of crack density (ε) . An increment in crack density reduces the velocities of faster (P_1, SV) waves, which implies that faster waves may slow down with the

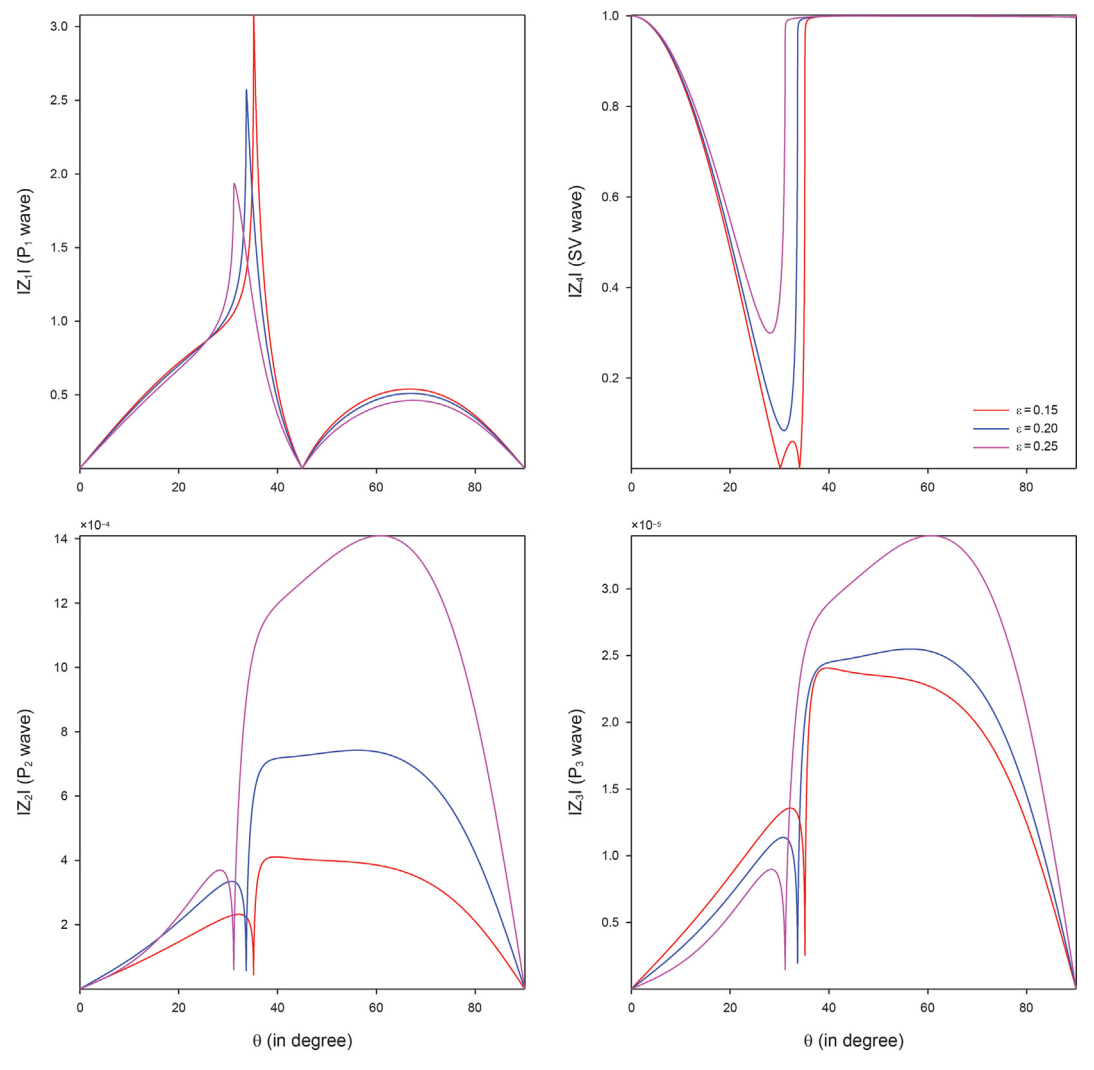


Fig. 9. Amplitude ratios $(|Z_1|, |Z_2|, |Z_3|, |Z_4|)$ of reflected waves; $\omega = 2\pi \times 300$ Hz; $R_0 = 0.0053$ m; $\gamma^* = 0.003$; $\gamma_b = 0.3$; $\gamma_0 = 45^\circ$; Incident SV wave.

increment in ε . In case of slower (P_2, P_3) waves, velocity of P_2 wave enlarges with the increment in ε and on contrary, P_3 wave may slow down a bit with the increment of ε . However, the decrement of velocities of faster waves (i.e., P_1 , SV) is very high as compared to the decrement of velocity of slower P_3 wave. An increment in ε reduces (enlarges) the attenuation of P_1 , P_3 (P_2 , SV) waves. The fast (slow) waves attenuate more (less). Fig. 2 displays effect of crack radius (R_0) on phase velocities and attenuation coefficients. Impact of R_0 is not noticed on the velocity and attenuation of fast SV wave. But, R_0 has a little effect on the velocity of fast P_1 wave. On the contrary, slower waves propagation characteristics (velocity/ attenuation) have a strong dependence on the size of inclusions as well as wave frequency. Fig. 3 illustrates the influence of crack aspect ratio (γ^*) on the phase velocities and attenuation coefficients of P_1, P_2, P_3 , SV waves with frequency. This figure clearly shows that the propagation characteristics of every wave have a strong dependence on the crack aspect ratio. Quite similar to Fig. 1, the velocities of faster waves reduces with the increment in the value of γ^* . Faster waves are highly perceptive to the crack aspect ratio of the penny-shaped inclusions. An increment in γ^* may enlarge the attenuation of faster waves. But, attenuation of slower $P_2(P_3)$ waves enlarges (reduces) with the increment in γ^* . Another

major parameter that can affect the wave propagation in cracked porous solid is the Poisson's ratio v_b . The variation of phase velocities and attenuation coefficients of P_1, P_2, P_3 , SV waves with ν_b are displayed in Fig. 4. As perceived from figure, with the increase of v_h , velocities of P_1 , SV waves increase significantly, whereas slower P_2 wave experiences a slight increase in velocity. This implies that increase in v_h strongly speeds up the faster waves. But, increase in v_h does not upset the velocity of P_3 wave and attenuation coefficient of SV wave much. From the comparison of plots in Figs. 1, Figs. 3 and 4, it is perceived that with the increase of ε and γ^* , faster waves significantly slow down while with the increase in v_b , these waves are strongly speeded up. Fig. 5 exhibits the impact of WIFF on $\alpha_1, \alpha_2, \alpha_3, \alpha_4$ and $\beta_1, \beta_2, \beta_3, \beta_4$ with frequency. It is clearly evident from this figure, the ubiquity of WIFF reduces the velocities as well as attenuation coefficients of longitudinal waves. But, the ubiquity of WIFF does not upset the velocity/attenuation of shear

6.2. Effect of various parameters on the reflection coefficients

6.2.1. Incident P_1 wave

Fig. 6 exhibits the impact of WIFF on the amplitude ratios ($|Z_1|$,

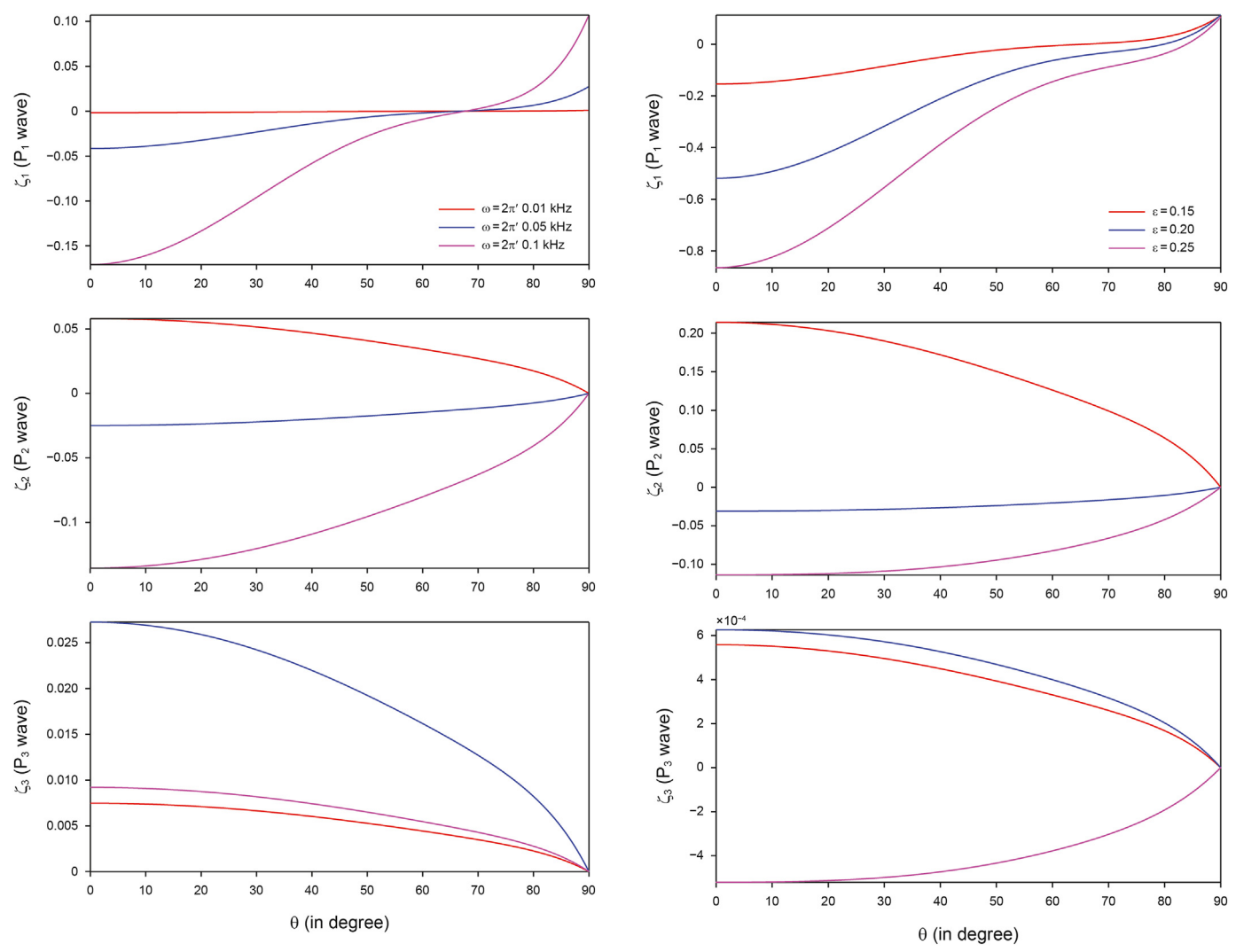


Fig. 10. Effect of wave frequency on the WIFF; $\varepsilon=0.15$; $x_3=0.9$ m; $R_0=0.0053$ m; $\gamma^*=0.003$; $v_b=0.3$; $\gamma_0=55^0$; Incident P_1 wave.

Fig. 11. Effect of crack density on the WIFF; $\omega=2\pi\times 100$ kHz; $x_3=0.9$ m; $R_0=0.007$ m; $\gamma^*=0.002$; $\nu_b=0.3$; $\gamma_0=45^0$; Incident P_1 wave.

 $|Z_2|$, $|Z_3|$, $|Z_4|$) of the reflected waves. A minute impact of WIFF is perceived on the behavior of P_1 wave. But, shear wave is not affected by the ubiquity of WIFF. The slower waves are strengthened a lot in the absence of WIFF. It means ubiquity of WIFF weakens the reflection capabilities of slower waves. The effect of crack density on $|Z_1|$, $|Z_2|$, $|Z_3|$, $|Z_4|$ with incident direction θ are displayed in Fig. 7. An increment in crack density strongly enlarges the reflection capability of P_1 wave. But, reflection capability of SV wave may weaken with the increment of crack density. A substantial impact of crack density is perceived at the normal incidences of P_2 and P_3 waves. However, at both grazing and normal incidences, faster waves are not perceptive to the alteration in crack density.

6.2.2. Incident SV wave

Fig. 8 shows the influence of WIFF on the amplitude ratios of the reflected waves. The P_1 wave is strongly strengthened in the ubiquity of WIFF near SV wave critical incidence. But, a minute impact of WIFF is perceived on shear wave near critical incidence. Critical angles are perceived for both P_1 (around 44^0) and SV (around 33^0) waves. The slower waves are strengthened considerably in the absence of WIFF. It means ubiquity of WIFF weakens the reflection

capabilities of slower waves. The effect of crack density on the amplitude ratios with incident direction θ is displayed in Fig. 9. A substantial impact of crack density is perceived on the P_1 wave for $23^0 < \theta < 40^0$ and a slightly less impact is seen for $50^0 < \theta < 80^0$. But, reflection capability of SV wave may strengthen with the increase of crack density for $22^0 < \theta < 39^0$. A substantial impact of crack density is perceived on the P_2 and P_3 waves. However, near both normal and grazing incidences, all the waves are not perceptive to the alteration in crack density.

6.3. Effect of various parameters on the wave-induced fluid flow

6.3.1. Incident P_1 wave

The WIFF of longitudinal waves (ς_k , k=1,2,3), reflected from the sealed-pore stress-free surface of cracked porous solid containing penny-shaped inclusions, are computed with incident directions (θ) for distinct values of wave frequency (ω), key parameters of cracks and distance from boundary. The variations of ς_k with frequency is shown in Fig. 10. From this figure it can be inferred that the significant contributors to the fluid flow are P_1 and P_2 waves. The enrichment of P_1 wave to the fluid flow enlarges with

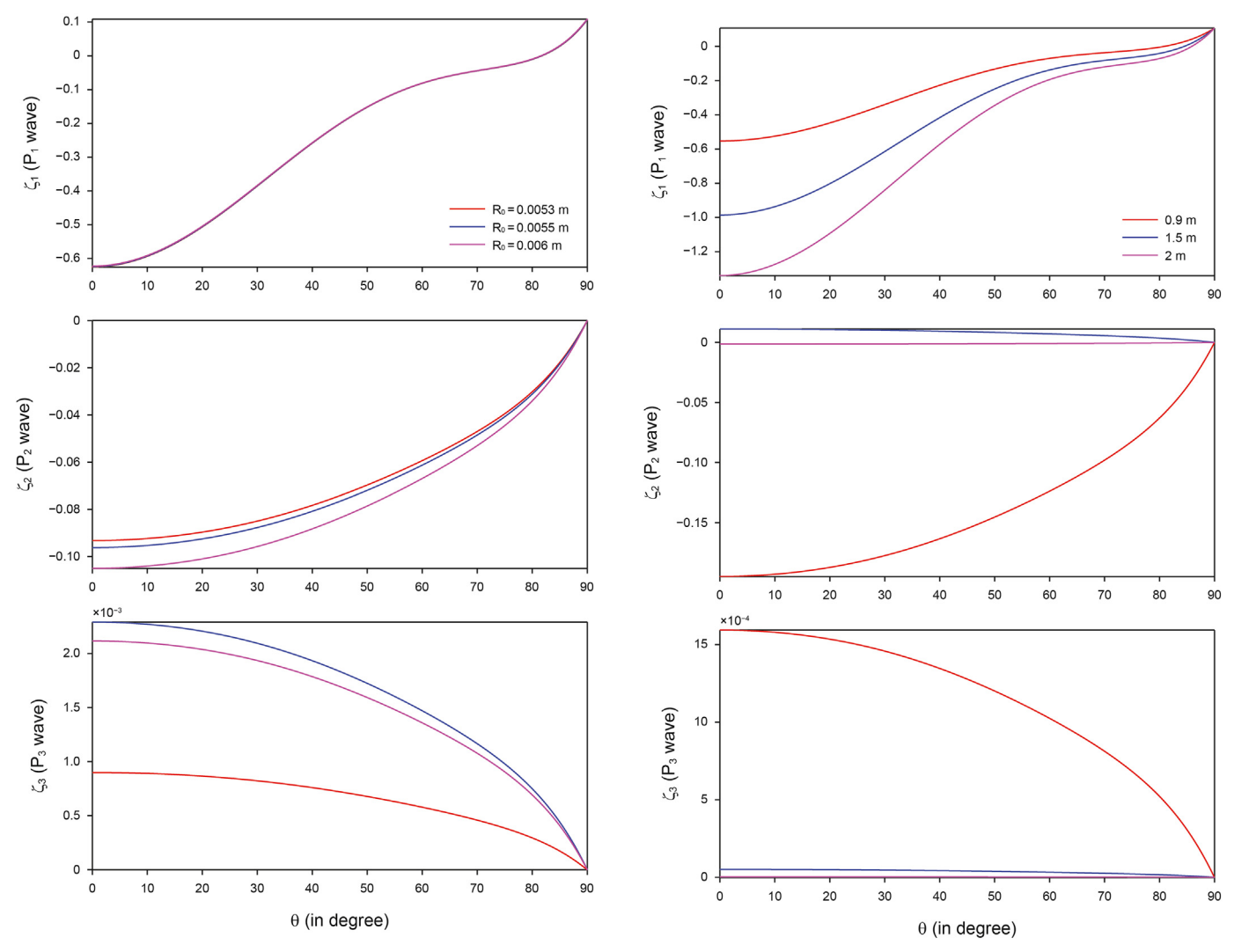


Fig. 12. Effect of crack radius on the WIFF; $\omega=2\pi\times 100$ kHz; $\varepsilon=0.2$; $x_3=1$ m; $\gamma^*=0.003$; $\nu_b=0.3$; $\gamma_0=45^0$; Incident P_1 wave.

Fig. 13. Effect of depth on the WIFF; $\omega=2\pi\times 100$ kHz; $\varepsilon=0.2$; $R_0=0.0053$ m; $\gamma^*=0.003$; $\nu_b=0.3$; $\gamma_0=45^0$; Incident P_1 wave.

the increment in frequency. Fluid flow induced by P_1 wave may disappear at lower frequency, especially, when $\omega = 0.01 \text{kHz}$. It reduces (enlarges) with the increment (decrement) in θ , specifically, for $\theta \le 70^0 (\theta > 70^0)$. However, contribution of P_2 wave reduces with the increment of incident angle. The fluid flow induced by P_3 wave enlarges (reduces) with the increment (decrement) in frequency (θ). The fluid flow induced by P_2 and P_3 waves disappear for incidence approaching the grazing direction. On contrary, fluid flow induced by P_1 wave does not disappear at this incidence. The WIFF of all the longitudinal waves may be highly perceptive to the alteration in wave frequency. Fig. 11 displays the variations of ς_k with crack density. It is clearly visible that crack density significantly influences the WIFF. The fluid flow induced by P_1 wave enlarges with the increment in crack density. It reduces with the increment in θ . On the contrary, fluid flow induced by P_2 wave reduces with the increment in crack density. The contribution of P_3 wave to the fluid flow is much smaller as compared to contributions of P_1 and P_2 waves. Fig. 12 illustrates the effect of crack radius on the WIFF (ς_k , k=1, 2, 3). From this figure, it is quite clear that no impact of crack radius is perceived on the fluid flow of P_1 wave. But, fluid flow of P_2 enlarges slightly with the increase in crack radius

and it decreases with the increase in incident direction θ . From Figs. 11 and 12, it may be visualized that the contribution of the P_3 wave to the wave induced fluid flow is negligible.

The variations of ς_k with incident direction θ at different depth are displayed in Fig. 13. An increment in depth enlarges the fluid flow induced by the P_1 wave. But it may decrease the fluid flow induced by the P_2 wave. The contribution of P_2 wave to the WIFF disappears at higher depth (i.e., $x_3=2$ m). All longitudinal waves are highly perceptive to alteration in depth. The variations of ς_k with incident direction θ at different aspect ratios are exhibited in Fig. 14. From the comparison of plots in this figure, it is perceived that the impact of γ^* is certainly stronger on the fluid flow induced by the P_2 and P_3 waves than that of P_1 wave. It means these waves are highly perceptive to the alteration in γ^* . The impact of γ^* on the wave induced flow of P_1 wave is perceived for $\theta \leq 45^0$.

6.3.2. Incident SV wave

The variations of ς_k for incident *SV* wave with frequency is shown in Fig. 15. A large contribution of P_1 to the fluid flow is perceived for $\theta > 30^0$. The contribution of P_1 wave to the fluid flow may disappear for $\theta \le 30^0$. Moreover, fluid flow induced by P_1 wave

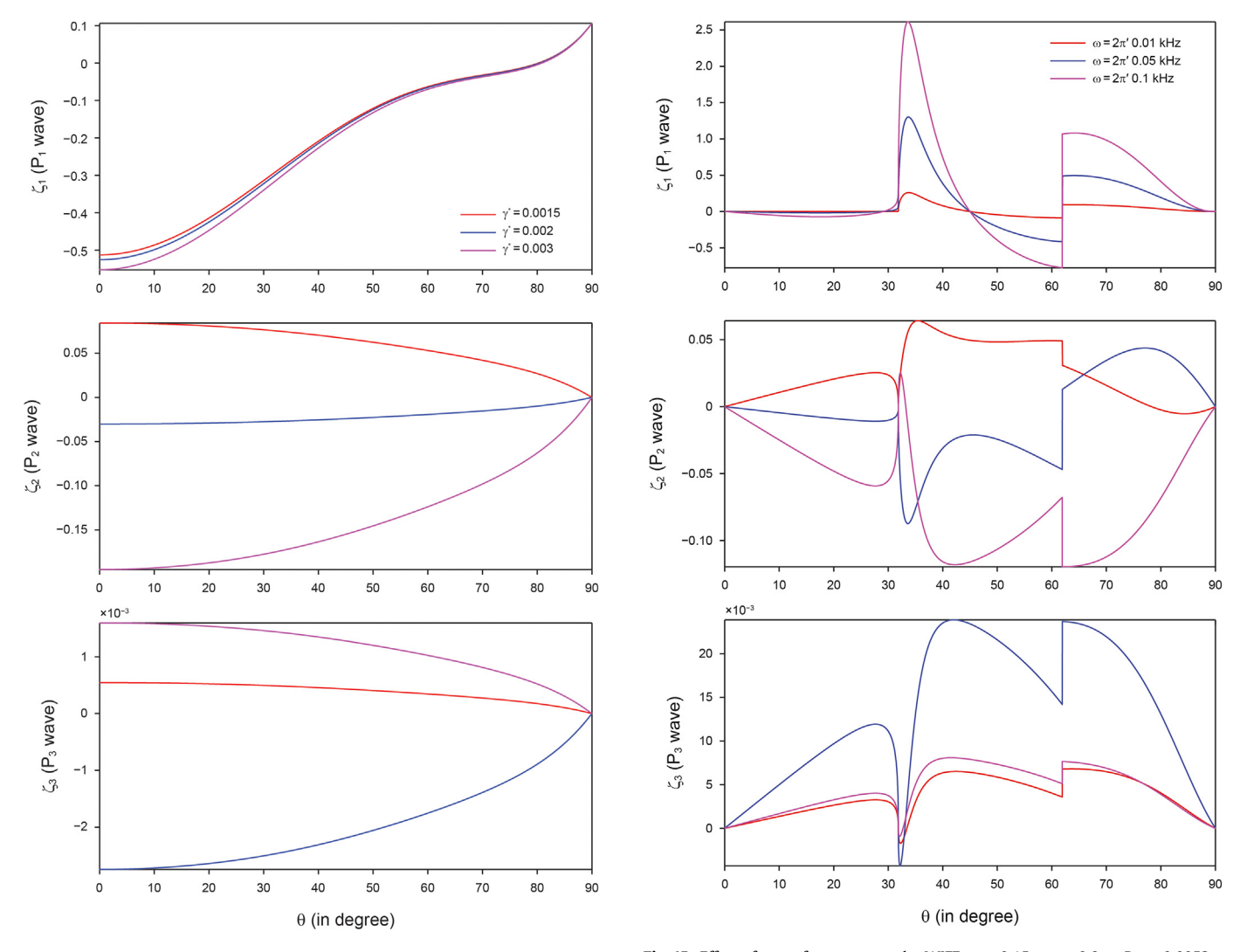


Fig. 14. Effect of crack aspect ratio on the WIFF; $\omega = 2\pi \times 100$ kHz; $\varepsilon = 0.2$; $x_3 = 0.9$ m; $R_0 = 0.0053$ m; $v_b = 0.3$; $\gamma_0 = 45^{\circ}$; Incident P_1 wave.

Fig. 15. Effect of wave frequency on the WIFF; $\varepsilon=0.15$; $x_3=0.9$ m; $R_0=0.0053$ m; $\gamma^*=0.003$; $\nu_b=0.3$; $\gamma_0=55^0$; Incident *SV* wave.

may disappear at lower frequency, especially, when $\omega = 0.01 \text{kHz}$. Further, from the plots of this figure, two specific directions are perceived; one near $\theta = 33^{\circ}$ and other near $\theta = 60^{\circ}$, where WIFF may enhance rapidly. Similar to Fig. 10 (incident P_1 wave), a substantial contribution of P_2 wave to fluid flow is also found for the incident SV wave. The contribution of P_3 wave enlarges with the increment in frequency for the entire range of θ . The fluid flow induced by these waves disappears at both normal and grazing incidences. Again, analogous to Fig. 10, WIFF of all the longitudinal waves may be highly perceptive to the alteration in wave frequency. Fig. 16 displays the variations of ς_k with incident direction θ at three different values of crack density. It is clearly visible that crack density significantly influences the WIFF. The fluid flow induced by P_1 wave is significantly affected by the crack density for $\theta > 30^{\circ}$. But, fluid flow induced by slower waves is significantly influenced by the crack density in the entire range of θ . The contribution of the P_3 wave to the fluid flow is negligible as compared to contributions

of P_1 and P_2 waves. Fig. 17 illustrates the effect of crack radius on the WIFF (ς_k , k=1,2,3). The impact of crack radius is not perceived on the fluid flow of P_1 wave. But, the fluid flow of P_2 enlarges slightly with the increment in crack radius for $\theta > 38^0$ and it enlarges significantly for $38^0 < \theta$. Analogous to the case of incident P_1 wave in Fig. 12, it is again visualized from the plots in this figure that the contribution of the P_3 wave to the wave induced fluid flow is negligible. The variations of ς_k with incident direction θ at different depth are displayed in Fig. 18. An increment in depth enlarges the fluid flow induced by the P_1 wave. However, a little impact of depth is perceived on it for $30^0 < \theta < 53^0$. Little bit contribution of P_2 wave to the wave-induced fluid is perceived for $x_3 = 1.5$ m and it disappears at higher depths (i.e., $x_3 = 2$ m). The behavior of P_3 wave at the depths $x_3 = 1.5$ m and $x_3 = 2$ m is quite similar to P_2 wave. Fig. 19 displays the variations of ς_k with incident direction θ at three different values of aspect ratio. The WIFF of P_1 wave may disappear

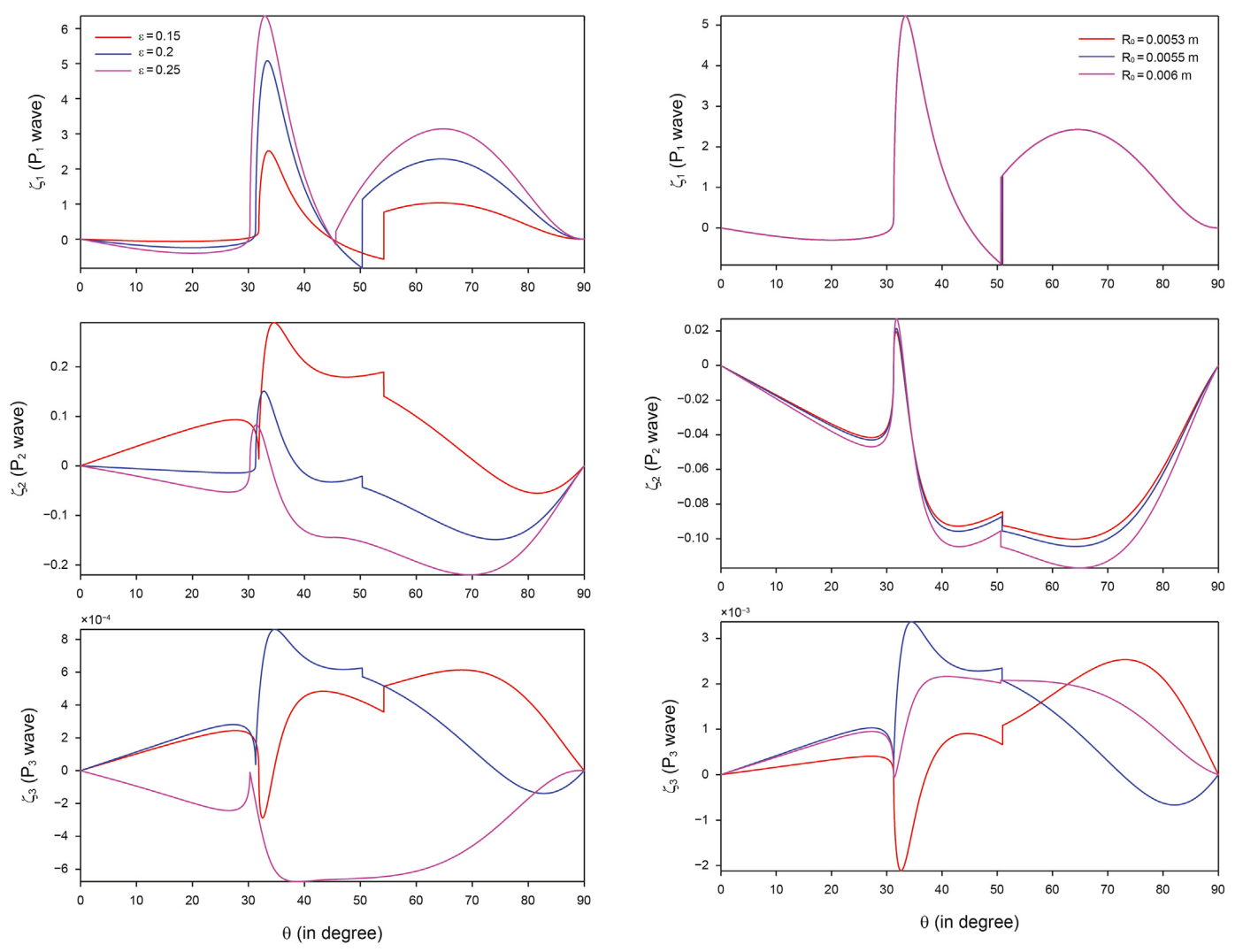


Fig. 16. Effect of crack density on the WIFF; $\omega=2\pi\times 100$ kHz; $x_3=0.9$ m; $R_0=0.007$ m; $\gamma^*=0.003$; $\nu_b=0.3$; $\gamma_0=45^0$; Incident SV wave.

Fig. 17. Effect of crack radius on the WIFF; $\omega=2\pi\times 100$ kHz; $\varepsilon=0.2$; $x_3=1$ m; $\gamma^*=0.003$; $v_b=0.3$; $\gamma_0=45^0$; Incident SV wave.

for all values of aspect ratios in the range of $\theta \in [0, 30^0]$. A little impact of γ^* on the wave induced flow of P_1 wave is perceived for $48^0 < \theta < 55^0$. From the comparison of plots in this figure, it is perceived that the impact of γ^* is certainly stronger on the fluid flow induced by the P_2 and P_3 waves than that of P_1 wave. It means these waves are highly perceptive than P_1 wave to the alteration in γ^* .

7. Conclusions

The key objective of this investigation is to analyze the wave characteristics (velocity/attenuation), reflection coefficients and WIFF in the cracked porous solid containing penny-shaped inclusions. In particularly, the contribution of longitudinal waves to WIFF is derived analytically and analyzed numerically with the help of specific numerical example. The effects of three key factors (crack density, crack radius, crack aspect ratio) of penny-shaped

cracked inclusions, depth and wave frequency are analyzed on contribution of fluid flow induced by the longitudinal waves. We have analytically showed that the fluid flow induced by each longitudinal wave is linked directly to its reflection coefficient. Some conclusions are addressed which may be drawn from the discussions of the numerical results.

1. The presence of cracks in the porous rock can notably reduce the elastic modulli of the rock. The influence of crack on the elastic wave propagation is accounted through crack-dependent dry bulk modulus. Overall, the influence of cracks is assimilated by considering three main factors of crack solid and these factors are crack density, crack radius and crack aspect ratio. The crack development is directly proportionate to the crack density (Shekhar and Parvez, 2016). The inverse impact of crack density is perceived on the faster waves (*P*₁ and *SV*). This implies that the crack growth slows down the faster waves.

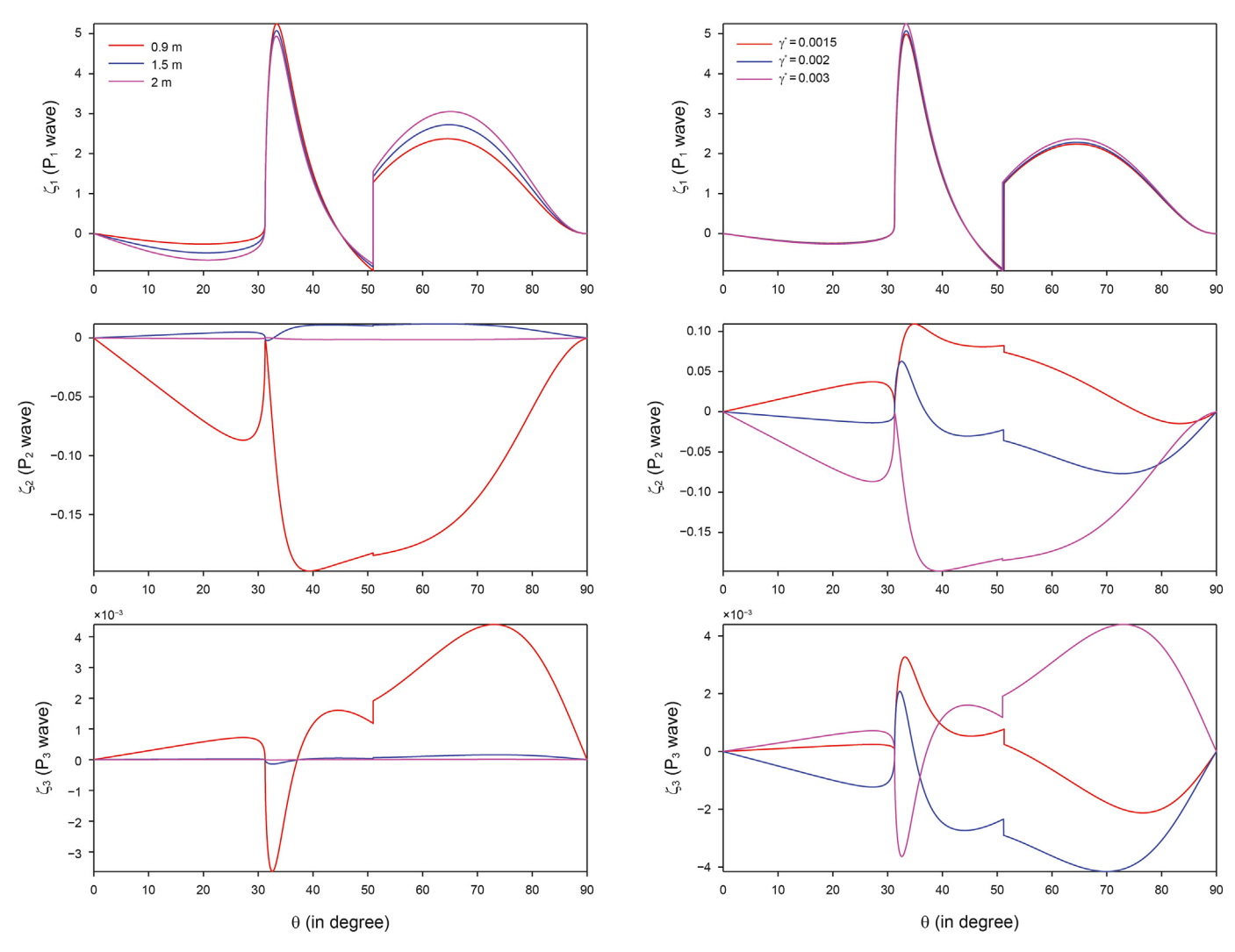


Fig. 18. Effect of depth on the WIFF; $\omega=2\pi\times 100$ kHz; $\varepsilon=0.2$; $R_0=0.0053$ m; $\gamma^*=0.003$; $\nu_b=0.3$; $\gamma_0=45^0$; Incident SV wave.

Fig. 19. Effect of crack aspect ratio on the WIFF; $\omega=2\pi\times 100$ kHz; $\varepsilon=0.2$; $x_3=0.9$ m; $R_0=0.0053$ m; $v_b=0.3$; $\gamma_0=45^0$; Incident *SV* wave.

- 2. An increase in crack aspect ratio (Poisson's ratio) rapidly slow down the faster waves. The P_1 wave is quite sensitive to crack radius but shear wave is not sensitive.
- 3. A remarkable impact of crack parameters, Poisson's ratio, WIFF and wave frequency is perceived on the velocities and attenuation coefficients of slower waves except on the velocity of P_3 wave which is not perceptive to v_b .
- 4. The attenuation coefficient of shear wave is not affected by crack radius, Poisson's ratio and WIFF. The WIFF has no impact on the *SV* wave but in the presence of WIFF, the longitudinal waves slow down rapidly i.e. velocities of these waves significantly decrease in the ubiquity of WIFF.
- 5. It is found analytically as well as graphically (Fig. 5) that shear wave does not impart to the WIFF. Therefore, fluid flow is induced only due to the propagation of longitudinal waves.
- 6. The reflection capabilities of slower waves are weakened in the presence of WIFF. For incident P_1 wave, reflection capability of P_1 (SV) wave enlarges (reduces) with the increment (decrement) in crack density.
- A significant impact of crack density is observed on the slower waves for both incident waves.

- 8. For the incidence of SV wave, the critical angle is found for P_1 (SV) waves.
- 9. The P_1 and P_2 waves induce more fluid flow, when the incidence of SV wave is considered. The fluid flow induced by the P_1 wave is not affected by the variations of two crack parameters-crack radius and aspect ratio, for the incidence of both P_1 and SV waves. The contribution of P_2 wave to the WIFF disappears at higher depth (i.e., $x_3 = 2$ m) for both cases. The contribution of P_3 wave is negligible. Compared to P_1 wave, the fluid flow induced by the P_2 and P_3 waves are highly sensitive to crack density, crack radius and crack aspect ratio. The positive value ς_k represents the flow of pore from the host medium to the penny-shaped inclusions.

Finally, an analysis of wave characteristics (velocity/attenuation), reflection coefficients and WIFF in cracked porous solid can facilitate to understand some scientific issues in exploration geophysics and seismology. The wave characteristics (velocity/attenuation) are mostly used to analyze the subsurface fluid movement. This study may play an important role in probe of prospects the oil/gas deposits in the cracked porous solid. The

resolution of various crack characteristics (i.e., crack density, crack radius and aspect ratio) and flow characteristics of the cracked porous solid are dependent on the knowledge of poroelastic reflection signatures. The knowledge of these aspects may be helpful in seismic evaluation and reservoir portrayal.

References

- Aggarwal, Y.P., Sykes, L.R., Armbruster, J., Sbar, M.L., 1973. Premonitory changes in seismic velocities and prediction of earthquakes. Nature 241, 101–104.
- Ba, J., Carcione, J.M., Nie, J.X., 2011. Biot-Rayleigh theory of wave propagation in double-porosity media. J. Geophys. Res. Solid Earth 116, B06202.
 Ba, J., Carcione, J.M., Sun, W., 2015. Seismic attenuation due to heterogeneities of
- Ba, J., Carcione, J.M., Sun, W., 2015. Seismic attenuation due to heterogeneities of rock fabric and fluid distribution. Geophys. J. Int. 202 (3), 1843–1847.
- Ba, J., Xu, W., Fu, L.Y., Carcione, J.M., Zhang, L., 2017. Rock anelasticity due to patchy saturation and fabric heterogeneity: a double double-porosity model of wave propagation. J. Geophys. Res. Solid Earth. 122 (3), 1949—1976.
- Barak, M.S., Kumari, M., Kumar, M., 2018. Effect of local fluid flow on the propagation of plane waves at an interface of water/double-porosity solid with underlying uniform elastic solid. Ocean. Eng. 147, 195—205.
- Biot, M.A., 1956a. Theory of propagation of elastic waves in fluid-saturated porous solid -Part 1: low frequency range. J. Acoust. Soc. Am. 28, 168–178.
- Biot, M.A., 1956b. The theory of propagation of elastic waves in a fluid-saturated porous solid, I. Low-frequency range, II. Higher frequency range. J. Acoust. Soc. Am. 28, 168–191.
- Biot, M.A., 1962a. Mechanics of deformation and acoustic propagation in porous media. J. Appl. Phys. 33, 1482–1498.
- Biot, M.A., 1962b. Generalized theory of acoustic propagation in porous dissipative media. J. Acoust. Soc. Am. 34, 1254–1264.
- Borcherdt, R.D., 2009. Viscoelastic Waves in Layered Media. Cambridge University Press. New York.
- Budiansky, B., O'Connell, R.J., 1976. Elastic moduli of a cracked solid. Int. J. Solid Struct. 12, 81–97.
- Budiansky, B., O'Connell, R.J., 1980. Bulk dissipation in heterogeneous media. Solid Earth Geophys Geotech 42, 1–10.
- Cheng, C.H., Toksöz, M.N., 1979. Inversion of seismic velocities for the pore aspect ratio spectrum of a rock. J. Geophys. Res. Solid Earth. 84, 7533—7543.
- David, E.C., Zimmerman, R.W., 2011. Compressibility and shear compliance of spheroidal pores: exact derivation via the Eshelby tensor, and asymptotic expressions in limiting cases. Int. J. Solid Struct. 48, 680–686.
- David, E.C., Zimmerman, R.W., 2012. Pore structure model for elastic wave velocities in fluid-saturated sandstones. J. Geophys. Res. Solid Earth. 117, B07210.
- Dvorkin, J., Nur, A., 1993. Dynamic poroelasticity: a unified model with the squirt and the Biot mechanisms. Geophysics 58, 524–533.
- Eshelby, J.D., 1957. The determination of the elastic field of an ellipsoidal inclusion, and related problems. Proc. Roy. Soc. Lond. A241 (1226), 376–396.
- and related problems. Proc. Roy. Soc. Lond. R241 (1226), 3/6–396.

 Galvin, R.J., Gurevich, B., 2009. Effective properties of a poroelastic medium con-
- taining a distribution of aligned cracks. J. Geophys. Res. Solid Earth. 114, B7. Garvin, H.D., Knopoff, 1973. The compressional modulus of a material permeated by a random distribution of circular cracks. Q. Appl. Math. 30, 453–464.
- Garvin, H.D., Knopoff, 1975aa. The shear modulus of a material permeated by a random distribution of free circular cracks. Q. Appl. Math. 33, 296–300.
- Garvin, H.D., Knopoff, 1975ba. Elastic moduli of a medium with liquid filled cracks. Q. Appl. Math. 33, 301–303.
- Gassmann, F., 1951. Über die Elastizität poröser Medien. Vierteljahrsschrift der Naturforschenden Gesellschaft Zürich 96, 1–23.
- Guo, J., Rubino, J.G., Glubokovskikh, S., Gurevich, B., 2017. Effects of fracture intersections on seismic dispersion: theoretical predictions versus numerical simulations. Geophys. Prospect. 65, 1264–1276.
- Gurevich, B., Brajanovski, M., Galvin, R.J., Müller, T.M., Toms-Stewart, J., 2009. P-wave dispersion and attenuation in fractured and porous reservoirs -Poroelasticity approach. Geophys. Prospect. 57, 225–237.
- Jakobsen, M., Hudson, J.A., Johansen, T.A., 2003. T-matrix approach to shale

- acoustics. Geophys. J. Int. 154, 533-558.
- Khalid, P., Ahmed, N., 2016. Modulus defect, velocity dispersion and attenuation in partially-saturated reservoirs of Jurassic sandstone, Indus basin, Pakistan. Studia Geophys. Geod. 60, 112–129.
- Kumar, M., Barak, M.S., Kumari, M., 2019. Reflection and refraction of plane waves at the boundary of an elastic solid and double-porosity dual-permeability materials. Petrol. Sci. 16, 298–317.
- Kumar, M., Kumari, M., Barak, M.S., 2018. Reflection of plane seismic waves at the surface of double-porosity dual-permeability materials. Petrol. Sci. 15, 521–537.
- Kumar, M., Sharma, M.D., 2013. Reflection and transmission of attenuated waves at the boundary between two dissimilar poroelastic solids saturated with two immiscible fluids. Geophys. Prospect. 61 (5), 1035—1055.
- Kumari, M., Kumar, M., 2020. Reflection of Inhomogeneous Waves at the Surface of a Cracked Porous Solid with Penny-Shaped Inclusions, vols. 1–22. Waves Random Complex Media.
- Kumari, M., Kumar, M., Barak, M.S., 2019. Wave Propagation Characteristics at the Welded Interface of Double-Porosity Solid and Double-Porosity Dual-Permeability Materials. Waves Random Complex Media, pp. 1–26.
- Mavko, G., Nur, A., 1975. Melt squirt in the aesthenosphere. J. Geophys. Res. 80, 1444–1448.
- Mavko, G., Nur, A., 1979. Wave attenuation in partially saturated rocks. Geophysics 44, 161–178.
- Murphy, W.F., Winkler, K.W., Kleinberg, R.L., 1986. Acoustic relaxation in sedimentary rocks, dependence on grain contacts and fluid saturation. Geophysics 51, 757–766.
- Müller, T.M., Gurevich, B., Lebedev, M., 2010. Seismic wave attenuation and dispersion resulting from wave-induced flow in porous rocks-A review. Geophysics 75 (5), 75A147—75A164.
- Nur, A., 1972. Dilatancy, pore fluids and premonitory variations of ts/tp travel times. Bull. Seismol. Soc. Am. 62, 1217–1222.
- O'Connell, R.J., Budiansky, B., 1974. Seismic velocities in dry and saturated cracked solids. J. Geophys. Res. 79, 4626–4627.
- O'Connell, R.J., Budiansky, B., 1977. Viscoelastic properties of fluid saturated cracked solids. J. Geophys. Res. 82, 5719–5736.
- Pride, S.R., Berryman, J.G., Harris, J.M., 2004. Seismic attenuation due to wave induced flow. J. Geophys. Res. 109, B01201.
- Quintal, B., Schmalholz, S.M., Podladchikov, Y.Y., 2011. Impact of fluid saturation on the reflection coefficient of a poroelastic layer. Geophysics 76 (2), N1–N12.
- Rayleigh, L., 1917. On the pressure developed in a liquid during the collapse of a spherical cavity. Phil. Mag. 34, 94–98.
- Shapiro, S.A., 2003. Elastic piezo sensitivity of porous and fractured rocks. Geophysics 68, 482–486.
- Shekhar, S., Parvez, I.A., 2016. Reflection and refraction of attenuated waves at the interface between cracked poroelastic medium and porous solid saturated with two immiscible fluids. Transport Porous Media 113, 405–430.
- Tang, X., 2011. A unified theory for elastic wave propagation through porous media containing cracks-An extension of Biot's poroelastic wave theory. Sci. China Earth Sci. 54, 1441–1452.
- Tang, X.M., Chen, X.L., Xu, X.K., 2012. A cracked porous medium elastic wave theory and its application to interpreting acoustic data from tight formations. Geophysics 77 (6), D245–D252.
- Thomsen, L., 1985. Biot-consistent elastic moduli of porous rocks: low-frequency limit. Geophysics 50, 2797–2807.
- Tran, D.T., Rai, C.S., Sondergeld, C.H., 2008. Changes in crack aspect ratio concentration from heat treatment: a comparison between velocity inversion and experimental data. Geophysics 73 (4), E123–E132.
- Walsh, J.B., 1965. The effect of cracks on the compressibility of rock. J. Geophys. Res. 70 (2), 381–389.
- Yao, Q., Han, D.H., Yan, F., Zhao, L., 2015. Modeling attenuation and dispersion in porous heterogeneous rocks with dynamic fluid modulus. Geophysics 80 (3), D183–D194.
- Zhang, L., Ba, J., Carcione, J.M., Fu, L.Y., 2020. Differential poroelasticity model for wave dissipation in self similar rocks. Int. J. Rock Mech. Min. Sci. 128, 104281.
- Zhang, L., Ba, J., Carcione, J.M., Sun, W., 2019. Modeling wave propagation in cracked porous media with penny-shaped inclusions. Geophysics 84 (4), 1–11.